



Nitrogen isotopic fractionations during nitric oxide production in an agricultural soil

Zhongjie Yu^{1,2} and Emily M. Elliott¹

¹Department of Geology and Environmental Science, University of Pittsburgh, Pittsburgh, Pennsylvania 15260, USA

²Department of Natural Resources and Environmental Sciences, University of Illinois Urbana-Champaign, Urbana, Illinois 61801, USA.

Correspondence to: Zhongjie Yu (zjyu@illinois.edu)

Abstract. Nitric oxide (NO) emissions from agricultural soils play a critical role in atmospheric chemistry and represent an important pathway for loss of reactive nitrogen (N) to the environment. With recent methodological advances, there is growing interest in the natural abundance N isotopic composition ($\delta^{15}\text{N}$) of soil-emitted NO and its utility in providing mechanistic information on soil NO dynamics. However, interpretation of soil $\delta^{15}\text{N}$ -NO measurements has been impeded by the lack of constraints on the isotopic fractionations associated with NO production and consumption in relevant microbial and chemical reactions. In this study, anoxic (0% O_2), oxic (20% O_2), and hypoxic (0.5% O_2) incubations of an agricultural soil were conducted to quantify the net N isotope effects ($^{15}\eta$) for NO production in denitrification, nitrification, and abiotic reactions of nitrite (NO_2^-) using a newly developed $\delta^{15}\text{N}$ -NO analysis method. A sodium nitrate (NO_3^-) containing mass-independent oxygen-17 excess (quantified by a $\Delta^{17}\text{O}$ notation) and three ammonium (NH_4^+) fertilizers spanning a $\delta^{15}\text{N}$ gradient were used in soil incubations to help illuminate the reaction complexity underlying NO yields and $\delta^{15}\text{N}$ dynamics in a heterogeneous soil environment. We found strong evidence for the prominent role of NO_2^- oxidation under anoxic conditions in controlling the apparent $^{15}\eta$ for NO production from NO_3^- in denitrification (i.e., 49 to 60‰). These results highlight the importance of an under-recognized mechanism for the reversible enzyme NO_2^- oxidoreductase to control the N isotope distribution between the denitrification products. Through a $\Delta^{17}\text{O}$ -based modeling of co-occurring denitrification and NO_2^- re-oxidation, the $^{15}\eta$ for NO_2^- reduction to NO and NO reduction to nitrous oxide (N_2O) were constrained to be 15 to 22‰ and -8 to 2‰, respectively. Production of NO in the oxic and hypoxic incubations was contributed by both NH_4^+ oxidation and NO_3^- consumption, with both processes having a significantly higher NO yield under O_2 stress. Under both oxic and hypoxic conditions, NO production from NH_4^+ oxidation proceeded with a large $^{15}\eta$ (i.e., 55 to 84‰) possibly due to expression of multiple enzyme-level isotopic fractionations during NH_4^+ oxidation to NO_2^- that involves NO as either a metabolic byproduct or an obligatory intermediate for NO_2^- production. Adding NO_2^- to sterilized soil triggered substantial NO production, with a relatively small $^{15}\eta$ (19‰). Applying the estimated $^{15}\eta$ values to a previous $\delta^{15}\text{N}$ measurement of in situ soil NO_x emission ($\text{NO}_x = \text{NO} + \text{N}_2\text{O}$) provided promising evidence for the potential of $\delta^{15}\text{N}$ -NO measurements in revealing NO production pathways. Based on the observational and modeling constraints obtained in this study, we suggest that simultaneous $\delta^{15}\text{N}$ -NO and $\delta^{15}\text{N}$ - N_2O measurements can lead to unprecedented insights into the sources of and processes controlling NO and N_2O emissions from agricultural soils.



1 Introduction

Agricultural production of food has required a tremendous increase in the application of nitrogen (N) fertilizers since the 1960s (Davidson, 2009). In order to maximize crop yields, N fertilizers are often applied in excess to agricultural soils, resulting in loss of reactive N to the environment (Galloway et al., 2003). Loss of N in the form of gaseous nitric oxide (NO) has long been recognized for its adverse impacts on air quality and human health (Veldkamp and Keller, 1997). Once emitted to the atmosphere, NO is rapidly oxidized to nitrogen dioxide (NO₂), and these compounds (collectively referred to NO_x) drive production and deposition of atmospheric nitrate (NO₃⁻) (Calvert et al., 1985) and play a critical role in the formation of tropospheric ozone (O₃) – a toxic air pollutant and potent greenhouse gas (Crutzen, 1979). Despite the observations that emission of NO from agricultural soils can sometimes exceed that of nitrous oxide (N₂O) – a climatically important trace gas primarily produced from reduction of NO in soils (Liu et al., 2017), NO is frequently overlooked in soil N studies due to its high reactivity and transient presence relative to N₂O (Medinets et al., 2015). Consequently, the contribution of soil NO emission to contemporary NO_x inventories at regional to global scales is highly uncertain (e.g., ranging from 3% to >30%) (Hudman et al., 2010; Vinken et al., 2014) and remains the subject of much current debate (Almaraz et al., 2018; Maaz et al., 2018).

As the “central hub” of the biogeochemical N cycle, NO can be produced and consumed in numerous microbial and chemical reactions in soils (Medinets et al., 2015). Among these processes, nitrification and denitrification are the primary sources responsible for NO emission from N-enriched agricultural soils (Firestone and Davidson, 1989). Denitrification is the sequential reduction of NO₃⁻ and nitrite (NO₂⁻) to NO, N₂O, and dinitrogen (N₂) and can be mediated by a diversity of soil heterotrophic microorganisms (Zumft, 1997). The enzymatic system of denitrification comprises a series of dedicated reductases whereby NO₂⁻ reductase (NIR) and NO reductase (NOR) are the key enzymes that catalyze production and reduction of NO, respectively (Ye et al., 1994). As such, NO is often viewed as a free intermediate of the denitrification process (Russow et al., 2009). In comparison, nitrification is a two-step aerobic process, in which oxidation of ammonia (NH₃) to NO₂⁻ is mediated by ammonia-oxidizing bacteria (AOB) or archaea (AOA), while the subsequent oxidation of NO₂⁻ to NO₃⁻ is performed by nitrite-oxidizing bacteria (NOB) (Lehnert et al., 2018). Although production of NO during the nitrification process has been linked to NH₃ oxidation (Hooper et al., 2005; Caranto et al., 2017) and NO₂⁻ reduction by AOB/AOA-encoded NIR (Wrage-Mönning et al., 2018), the metabolic role of NO in AOB and AOA remains ambiguous, making it difficult to elucidate the enzymatic pathways driving NO release by nitrification (Beckman et al., 2018; Stein, 2019). Additionally, NO can also be produced from abiotic reactions involving soil NO₂⁻ or its protonated form – nitrous acid (HNO₂) (Venterea et al., 2005; Lim et al., 2018). However, despite empirical evidence for the dependence of soil NO emission on soil N availability and moisture content (Davidson and Verchot, 2000), the source contribution of soil NO emission across temporal and spatial scales is poorly understood (Hudman et al., 2012). This is largely due to the lack of a robust means for source partitioning soil-emitted NO under dynamic environmental conditions.

Natural abundance stable N and oxygen (O) isotopes in N-containing molecules have long provided insights into the sources and relative rates of biogeochemical processes comprising the N cycle (Granger and



Wankel, 2016). The unique power of stable isotope ratio measurements stems from the distinct partitioning of isotopes between chemical species or phases, known as isotopic fractionation. Thus, in order to extract the greatest information from the distributions of isotopic species, a rigorous understanding of the direction and magnitude of isotopic fractionations associated with each relevant transformation is required. Both kinetic and equilibrium isotope effects can lead to isotopic fractionations between N-bearing compounds in soils (Granger and Wankel, 2016; Denk et al., 2017). During kinetic processes, isotopic fractionation occurs as a result of differences in the reaction rates of isotopically substituted molecules, leading to either enrichment or, in a few rare cases, depletion of heavy isotopes in the reaction substrate (Fry, 2006; Casciotti, 2009). The degree of kinetic fractionation can be quantified by a kinetic fractionation factor (α_k), which is often represented by the ratio of reaction rate constant of light isotopes to that of heavy isotopes. In this definition, α_k is larger than 1 for a normal kinetic fractionation. For equilibrium reactions, equilibrium fractionation arises from differences in the zero-point energies of two species undergoing isotopic exchange, leading to enrichment of heavy isotopes in the more strongly bonded form (Fry, 2006; Casciotti, 2009). In this case, the isotope ratios of two species at equilibrium are defined by an equilibrium fractionation factor (α_{eq}), which is also related to the kinetic fractionation factors of forward and backward equilibrium reactions (Fry, 2006). By convention, isotopic fractionation can be expressed in units of per mille (‰) as an isotope effect (ϵ): $\epsilon = (\alpha - 1) \times 1000$. Nevertheless, in a heterogeneous soil environment, expression of intrinsic kinetic and equilibrium isotope effects for biogeochemical N transformations is often limited due to transport limitation in soil substrates, the multi-step nature of transformation processes, as well as presence of diverse soil microbial communities that transform N via parallel and/or competing reaction pathways (Maggi and Riley, 2010). As such, interpretation of N isotope distribution in soils has largely relied on measuring net isotope effects (η), which are often characterized by incubating soil samples under environmentally relevant conditions, that favor expression of intrinsic isotope effects for specific N transformations (Lewicka-Szczepak et al. 2014). For example, it has been shown that the net N isotope effects for N₂O production in soil nitrification, denitrification, and abiotic reactions are distinctively different under certain soil conditions (Denk et al., 2017), rendering natural abundance N isotopes of N₂O a useful index for inferring sources of N₂O in agricultural soils (Toyoda et al., 2017).

While the isotopic dynamics underlying soil N₂O emissions has been extensively studied, there has been little investigation into the N isotopic composition (notated as $\delta^{15}\text{N}$ in units of ‰; $\delta = ((R_{\text{sample}}/R_{\text{standard}}) - 1) \times 1000$) of soil-emitted NO due to measurement difficulties (Yu and Elliott, 2017). Using a tubular denuder that trapped NO released from urea and ammonium (NH₄⁺)-fertilized soils, Li and Wang (2008) revealed a gradual increase in $\delta^{15}\text{N}$ -NO from -49 to -19‰ and simultaneous ¹⁵N enrichment in soil NH₄⁺ and NO₃⁻ over a two-week laboratory incubation. Similar $\delta^{15}\text{N}$ variations (i.e., -44 to -14‰) were recently reported for in situ soil NO_x emission in a manure-fertilized cornfield (Miller et al., 2018). Moreover, the magnitude of $\delta^{15}\text{N}$ -NO_x measured in this study depended on manure application methods, implying that NO_x was mainly sourced from nitrification of manure-derived NH₄⁺ (Miller et al., 2018). Based on a newly developed soil NO collection system that quantitatively converts soil-emitted NO to NO₂ for collection in triethanolamine (TEA) solutions, our previous work demonstrated substantial variations in $\delta^{15}\text{N}$ -NO (-54 to -37‰) in connection with changes in moisture content in a forest soil (Yu and Elliott, 2017). Furthermore, the measured in situ $\delta^{15}\text{N}$ -NO values spanned a wide range (-60 to -23‰) and were



110 highly sensitive to added N substrates (i.e., NH_4^+ , NO_3^- , and NO_2^-), indicating that NO produced from different sources may bear distinguishable $\delta^{15}\text{N}$ imprints (Yu and Elliott, 2017). Nevertheless, despite the potential of $\delta^{15}\text{N}$ -NO measurements in providing mechanistic information on soil NO dynamics, interpretation of $\delta^{15}\text{N}$ -NO has been largely impeded by the knowledge gap as to how $\delta^{15}\text{N}$ -NO is controlled by N isotopic fractionations during NO production and consumption in soils.

115 To this end, we conducted a series of controlled incubation experiments to quantify the net N isotope effects for NO production in an agricultural soil. Replicate soil incubations were conducted to measure the yield and $\delta^{15}\text{N}$ of soil-emitted NO under anoxic (0% O_2), oxic (20% O_2), and hypoxic (0.5% O_2) conditions, respectively. A sodium NO_3^- fertilizer mined in the Atacama Desert, Chile (Yu and Elliott, 2018) was used to amend the soil in all three incubation experiments. This Chilean NO_3^- originated from atmospheric deposition and thus contained an
120 anomalous ^{17}O excess (quantified by a $\Delta^{17}\text{O}$ notation) as a result of mass-independent isotopic fractionations during its photochemical formation in the atmosphere (Michalski et al., 2004). Because isotopic fractionations during biogeochemical NO_3^- production and consumption are mass-dependent, $\Delta^{17}\text{O}$ - NO_3^- is a conservative tracer of gross nitrification and NO_3^- consumption and provides a quantitative benchmark for disentangling isotopic overprinting on $\delta^{15}\text{N}$ - NO_3^- and $\delta^{18}\text{O}$ - NO_3^- during co-occurring nitrification and denitrification (Yu and Elliott, 2018) (see Text S1 in
125 the Supplement for more details). As additional tracers, three isotopically different NH_4^+ fertilizers were used in parallel treatments of the oxic and hypoxic incubations to quantify the source contribution of NO production with changing O_2 availability. By integrating multi-species measurements of N and O isotopes in an isotopologue-specific modeling framework, we were able for the first time to unambiguously link the yield and $\delta^{15}\text{N}$ variations of soil-emitted NO to nitrification and denitrification carried out by whole soil microbial communities and to
130 characterize the net isotope effects for NO production from soil NO_3^- , NH_4^+ , and NO_2^- under different redox conditions. The quantified isotope effects are discussed in the context of chemical and enzymatic pathways leading to net NO production in the soil environment and are applied to a previous field study (Miller et al., 2018) to provide implications for tracing the sources of NO emission from agricultural soils.

2 Materials and methods

135 2.1 Soil characteristics and preparation

Soil samples used in this study were collected in July 2017 from a conventional corn-soybean rotation field in central Pennsylvania, USA, managed by the USDA (Agricultural Research Service, University Park, PA, USA). The soil is a well-drained Hagerstown silt loam (fine, mixed, semiactive, mesic Typic Hapludalfs) with sand, silt, and clay content of 21%, 58%, and 21%, respectively. The sampled surface layer (0 - 10 cm) had a bulk density of 1.2
140 $\text{g}\cdot\text{cm}^{-3}$ and a pH (1:1 water) of 5.7. Total N content was 0.2% and $\delta^{15}\text{N}$ of total N was 5.3‰. Soil C:N ratio was 11.4 and organic carbon content was 1.8%. In the laboratory, soils were homogenized and sieved to 2 mm (but not air-dried) and then stored in resealable plastic bags at 4°C until further analyses and incubations. Gravimetric water content of the sieved and homogenized soils was 0.14 $\text{g H}_2\text{O}\cdot\text{g}^{-1}$. Indigenous NH_4^+ and NO_3^- concentrations were 0.7



145 $\mu\text{g N}\cdot\text{g}^{-1}$ and $19.8 \mu\text{g N}\cdot\text{g}^{-1}$, respectively. Throughout this paper, soil N concentrations, NO fluxes, and N transformation rates are expressed on the basis of soil oven-dry (105°C) weight.

2.2 Net NO production and collection of NO for $\delta^{15}\text{N}$ analysis

The recently developed soil dynamic flux chamber (DFC) system was used to measure net NO production rates and to collect soil-emitted NO for $\delta^{15}\text{N}$ analysis (Yu and Elliott, 2017). A schematic of the DFC system is shown in Fig. 1a. Detailed development and validation procedures for the NO collection method were presented in Yu and Elliott
150 (2017). Briefly, custom-made flow-through incubators modified from 1 L Pyrex medium bottles (13951L, Corning, USA) were used for all the incubation experiments (Fig. 1b). Each incubator was stoppered with two 42 mm Teflon septa secured by an open-topped screw cap and equipped with two vacuum valves for purging and closure of the incubator headspace. To measure net NO production from enclosed soil samples, a flow of NO-free air with desired O_2 content was directed through the incubator into a chemiluminescent NO- NO_x - NH_3 analyzer (model 146i, Thermo
155 Fisher Scientific) (Fig. 1a) (Yu and Elliott, 2017). Outflow NO concentration was monitored continuously until steady and then the net NO production rate was determined from the flow rate and steady-state NO concentration. To collect NO for $\delta^{15}\text{N}$ analysis, a subsample of the incubator outflow was forced to pass through a NO collection train (Fig. 1a) where NO is converted to NO_2 by excess O_3 (~ 3 ppm) in a Teflon reaction tube (9.5 mm I.D., ca. 240
160 cm length) and subsequently collected in a 500 mL gas washing bottle containing a 20% (v/v, 70 mL) TEA solution (Yu and Elliott, 2017). The collection products were about 90% NO_2^- and 10% NO_3^- (Yu and Elliott, 2017). Results from comprehensive method testing showed that the NO collection efficiency was $98.5\pm 3.5\%$ over a wide range of NO concentrations (12 to 749 ppb) and environmental conditions (e.g., temperature from 11 to 31°C and relative humidity of the incubator outflow from 27 to 92%) (Yu and Elliott, 2017). Moreover, it was confirmed that high concentrations of ammonia (NH_3) (e.g., 500 ppb) and nitrous acid (HONO) (removed by an inline HONO scrubber
165 (Fig. 1a)) in the incubator outflow do not interfere with NO collection (Yu and Elliott, 2017).

2.3 Anoxic incubation

To prepare for the anoxic incubation, the soil samples were spread out on a covered tray for pre-conditioning under room temperature (21°C) for 24 h. Next, the soil was amended with the Chilean NO_3^- fertilizer ($\delta^{15}\text{N}=0.3\pm 0.1\%$, $\delta^{18}\text{O}=55.8\pm 0.1\%$, $\Delta^{17}\text{O}=18.6\pm 0.1\%$) to achieve a fertilization rate of $35 \mu\text{g NO}_3^- \cdot \text{N}\cdot\text{g}^{-1}$ and a target soil water content of $0.21 \text{ g H}_2\text{O}\cdot\text{g}^{-1}$ (equivalent to 46% water-filled pore space (WFPS)). The fertilized soil samples were thoroughly homogenized using a glass rod in the tray. 100 g (dry weight equivalent) soil was then weighed into each of eight incubators, resulting in a soil depth of about 1.5 cm. The incubators were connected in parallel using a Teflon purging manifold (Fig. 1c), vacuumed and filled with ultra-purity N_2 for three cycles, and incubated in dark with a continuous flow of N_2 circulating through each of the eight incubators at 0.015 standard liter per minute
175 (SLPM). The sample fertilization and preparation procedures were repeated three times to establish three batches of replicate samples, leading to 24 soil samples in total for the anoxic incubation.

The first NO measurement and collection event was conducted 24 h after the onset of the anoxic incubation and daily sampling was conducted thereafter. At each sampling event, one incubator from each replicate sample



180 batch was isolated by closing the vacuum valves, removed from the purging manifold, and then measured using the DFC system. To prevent O₂ contamination by residual air in the DFC system, the DFC system was evacuated and flushed with N₂ five times before the vacuum valves were re-opened. A flow of N₂ was then supplied at 1 SLPM for continuous NO concentration measurement and collection. Samples from the replicate batches were measured successively.

185 Following the completion of measurement and collection of each sample, the incubator was opened from the top and the soil was combined with 500 mL deionized water for extraction of soil NO₃⁻ and NO₂⁻ (McKenney et al., 1982). Because NO₂⁻ accumulation was found in pilot experiments, deionized water, rather than routinely used KCl solutions, was used for the extraction to ensure accurate NO₂⁻ determination (Homyak et al., 2015). To extract soil NO₃⁻ and NO₂⁻, the soil slurry was agitated vigorously on a stir plate for 10 minutes and then centrifuged for 10 minutes at 2000 rpm. The resultant supernatant was filtered through a sterile 0.2 μm filter (Homyak et al., 2015). In
190 light of high NO₂⁻ concentrations observed in the pilot experiments, the filtrate was divided into two 60 mL Nalgene bottles, with one of the bottles receiving sulfamic acid to remove NO₂⁻ (Granger et al., 2009). This NO₂⁻-removed sample was used for NO₃⁻ isotope analysis, while the other sample without sulfamic acid treatment was used for determining NO₂⁻ and NO₃⁻ concentrations and combined δ¹⁵N analysis of NO₂⁻+NO₃⁻. Two important control tests, based on NO₂⁻/NO₃⁻ spiking and acetylene (C₂H₂) addition, were conducted to evaluate the robustness of the adopted
195 soil incubation and extraction methods. The results confirmed that the water extraction method was robust for determining concentrations and isotopic composition of soil NO₃⁻ and NO₂⁻ and that aerobic NO₃⁻ production from NH₄⁺ oxidation was negligible during the soil incubation and extraction procedures (Table S1 and Table S2; see Text S2 in the Supplement for more details).

2.4 Oxic and hypoxic incubations

200 The same pre-conditioning and fertilization protocol described for the anoxic incubation was used for the oxic and hypoxic incubations. Three isotopically different NH₄⁺ fertilizers were used in parallel treatments of each incubation experiment: (1) δ¹⁵N-NH₄⁺=1.9‰ (low ¹⁵N enrichment), (2) δ¹⁵N-NH₄⁺=22.5‰ (intermediate ¹⁵N enrichment), and (3) δ¹⁵N-NH₄⁺=45.0‰ (high ¹⁵N enrichment). An off-the-shelf ammonium sulfate ((NH₄)₂SO₄) reagent was used in the low δ¹⁵N-NH₄⁺ treatment, while the fertilizers with intermediate and high enrichment of ¹⁵N were prepared by
205 gravimetrically mixing the (NH₄)₂SO₄ reagent with NH₄⁺ reference materials IAEA-N2 (δ¹⁵N-NH₄⁺=20.3‰) and USGS26 (δ¹⁵N-NH₄⁺=53.7‰). In both oxic and hypoxic incubations, each of the three δ¹⁵N-NH₄⁺ treatments consisted of three replicate sample batches where each batch consisted of eight samples, resulting in 72 samples for each incubation experiment.

210 At the onset of each incubation experiment, soil samples (100 g dry weight equivalent) were amended with desired NH₄⁺ fertilizer (90 μg N·g⁻¹) and the Chilean NO₃⁻ fertilizer (15 μg N·g⁻¹) to the target soil water content of 0.21 g H₂O·g⁻¹ (46% WFPS). Following the amendment, two soil samples from each replicate batch were immediately extracted – one with 500 mL of deionized water for soil NO₂⁻ and NO₃⁻ using the extraction method described above and the other one with 500 mL of a 2 M KCl solution for determination of soil NH₄⁺. The remaining samples were incubated under desired O₂ conditions until further measurements. In the oxic incubation,



215 the incubators were connected in parallel using the purging manifold and continuously flushed by a flow of zero air
(20% O₂ + 80% N₂). In the hypoxic incubation, a flow of synthetic air with 0.5% O₂ content (balanced by 99.5% N₂)
was used to incubate the soil samples. The synthetic air was generated by mixing the zero air with ultra-purity N₂
using two mass flow controllers (Model SmartTrak 50, Sierra Instruments).

220 Replicate NO measurement and collection events were conducted at 24 h, 48 h, and 72 h following the
onset of the oxic and hypoxic incubations. Because net NO production rates were low under oxic and hypoxic
conditions, all remaining soil samples in each replicate batch were connected in parallel for NO measurement and
collection using the DFC system. This parallel connection ensured high outflow NO concentrations (i.e., >30 ppb)
required for quantitative NO collection (Yu and Elliott, 2017). The flow rate of purging air (20% O₂ for the oxic
incubation and 0.5% O₂ for the hypoxic incubation) during the DFC measurement was 0.25 SLPM to each
225 incubator. Following the NO measurement and collection, two soil samples from each replicate batch were extracted
for determination of soil NO₃⁻/NO₂⁻ (500 mL deionized water) and NH₄⁺ (500 mL 2M KCl), respectively. Because
NO concentrations were too low for reliable NO collection at 72 h after the onset of the incubations, only net NO
production rates were measured using the remaining two soil samples in each replicate batch.

2.5 Abiotic NO production

230 The potential for NO production from abiotic reactions was assessed using sterilized soil samples. Soil samples (100
g dry-weight equivalent) were weighed into the incubators and then autoclaved at 121°C and 1.3 atm for 30 minutes.
The autoclaved samples were pre-incubated under oxic and anoxic conditions, respectively, for 24 h and then
fertilized with the Chilean NO₃⁻ (35 µg NO₃⁻-N·g⁻¹) or the lab (NH₄)₂SO₄ (90 µg NH₄⁺-N·g⁻¹). The fertilizer
solutions were added to the soil surface through the Teflon septa using a sterile syringe equipped with a 25-gauge
235 needle. These samples were then measured periodically for net NO production. Because NO₂⁻ was found to
accumulate during the anoxic incubation (see below), four soil samples were sterilized, pre-incubated under anoxic
condition, and then fertilized with a NaNO₂ solution (δ¹⁵N-NO₂⁻=1.4±0.2‰) (8 µg N·g⁻¹) for immediate NO
measurement and collection. These NO₂⁻-amended samples were thereafter incubated under anoxic conditions and
measured periodically for net NO production until undetectable.

2.6 Chemical and isotopic analyses

240 Soil NO₃⁻ concentrations were determined using a Dionex Ion Chromatograph ICS-2000 with a precision of (1σ) of
±5.0 µg N·L⁻¹. Soil NO₂⁻ concentrations were analyzed using the Greiss-Islovay colorimetric reaction with a
precision of ±1.2 µg N·L⁻¹. Soil NH₄⁺ concentrations were measured using a modified fluorometric OPA method for
soil KCl extracts (Kang et al., 2003) with a precision of ±7.0 µg N·L⁻¹. NO₂⁻+NO₃⁻ concentration in the TEA
245 collection samples was measured using a modified spongy cadmium method with a precision of ±1.6 µg N·L⁻¹ (Yu
and Elliott, 2017).

The denitrifier method (Sigman et al., 2001; Casciotti et al., 2002) was used to measure δ¹⁵N and δ¹⁸O of
NO₃⁻ in the NO₂⁻-removed soil extracts and the δ¹⁵N of NO₃⁻+NO₂⁻ in the extracts without sulfamic acid treatment.
In brief, a denitrifying bacterium (*Pseudomonas aureofaciens*) lacking the N₂O reductase enzyme was used to



250 convert 20 nmol of NO_3^- into gaseous N_2O . The N_2O was then purified in a series of chemical traps, cryo-focused, and finally analyzed on a GV Instruments Isoprime Continuous Flow Isotope Ratio Mass Spectrometer (CF-IRMS) at m/z 44, 45, and 46 at the University of Pittsburgh *Regional Stable Isotope Laboratory for Earth and Environmental Science Research* where all isotope analyses were conducted for this study. International NO_3^- reference standards IAEA-N3, USGS34, and USGS35 were used to calibrate the $\delta^{15}\text{N}$ and $\delta^{18}\text{O}$ analyses. The long-
255 term precision is $\pm 0.3\text{‰}$ and $\pm 0.5\text{‰}$, respectively, for the $\delta^{15}\text{N}$ and $\delta^{18}\text{O}$ analyses. Because the denitrifier method does not differentiate NO_3^- and NO_2^- for the $\delta^{15}\text{N}$ analysis, $\delta^{15}\text{N}$ of NO_2^- was estimated using an isotopic mass balance when NO_2^- accounted for a significant fraction of the total $\text{NO}_3^- + \text{NO}_2^-$ pool.

$\Delta^{17}\text{O}$ of NO_3^- was measured using the coupled bacterial reduction and thermal decomposition method described by Kaiser et al. (2007). The denitrifying bacteria were used to convert 200 nmol of NO_3^- to N_2O , which
260 was subsequently converted to O_2 and N_2 by reduction over a gold surface at 800°C . The produced O_2 and N_2 were separated using a 5Å molecular sieve gas chromatograph, and the O_2 was then analyzed for $\delta^{17}\text{O}$ and $\delta^{18}\text{O}$ using the CF-IRMS. $\Delta^{17}\text{O}$ was calculated from the measured $\delta^{17}\text{O}$ and $\delta^{18}\text{O}$ using Equation (1) (see Text S1 in the Supplement) and calibrated by USGS34, USGS35, and a 1:1 mixture of USGS34 and USGS35.

$$\Delta^{17}\text{O} = \left[\ln \left(\frac{\delta^{17}\text{O}}{1000} + 1 \right) - 0.52 \ln \left(\frac{\delta^{18}\text{O}}{1000} + 1 \right) \right] \times 1000 \quad \text{Equation (1)}$$

265 The precision of the $\Delta^{17}\text{O}$ analysis of USGS35 and the USGS35:USGS34 mixture is $\pm 0.3\text{‰}$ (Yu and Elliott, 2018). Following Kaiser et al. (2007), the measured $\Delta^{17}\text{O}\text{-NO}_3^-$ was used in the reduction of molecular isotope ratios of N_2O to correct for the isobaric interference (i.e., m/z 45) on the measured $\delta^{15}\text{N}\text{-NO}_3^-$.

$\delta^{15}\text{N}$ of NH_4^+ in the KCl extracts was measured by coupling the NH_3 diffusion method (Zhang et al., 2015) and the hypobromite (BrO^-) oxidation method (Zhang et al., 2007) with the denitrifier method (Felix et al., 2013).
270 Briefly, an aliquot of soil KCl extract with 60 nmol NH_4^+ was pipetted into a 20 mL serum vial containing an acidified glass fiber disk. The solution was made alkaline by adding magnesium oxide (MgO) to volatilize NH_3 , which was subsequently captured on the acidic disk as NH_4^+ . After incubation under 37°C for 10 d, NH_4^+ was eluted from the disk using deionized water, diluted to $10\ \mu\text{M}$, oxidized by BrO^- to NO_2^- , and finally measured for $\delta^{15}\text{N}$ as NO_2^- at 20 nmol using the denitrifier method. International NH_4^+ reference standards IAEA-N1, USGS25, and
275 USGS26 underwent the same preparation procedure as the soil KCl extracts and were used along with the NO_3^- reference standards to correct for blanks and instrument drift. The precision of the $\delta^{15}\text{N}\text{-NH}_4^+$ analysis is $\pm 0.5\text{‰}$ (Yu and Elliott, 2018).

$\delta^{15}\text{N}$ of NO collected in the TEA solution was measured following the method described in Yu and Elliott (2017). Briefly, the TEA collection samples were first neutralized with 12 N HCl to pH ~ 7 , and then 10 to 20 nmol
280 of the collected product $\text{NO}_2^- + \text{NO}_3^-$ was converted to N_2O using the denitrifier method. In light of the low $\delta^{15}\text{N}$ values of soil-emitted NO and the presence of NO_2^- as the dominant collection product, a low $\delta^{15}\text{N}$ NO_2^- isotopic standard (KNO_2 , RSIL20, USGS Reston; $\delta^{15}\text{N} = -79.6\text{‰}$) was used together with the international NO_3^- reference standards to calibrate the $\delta^{15}\text{N}\text{-NO}$ analysis. Following the identical treatment principle, we prepared the isotopic standards in the same matrix (i.e., 20% TEA) as the collection samples and matched both the molar N amount and
285 injection volume ($\pm 5\%$) between the collection samples and the standards to minimize the blank interferences associated with the bacterial medium and the TEA solution. The precision and accuracy of the $\delta^{15}\text{N}\text{-NO}$ analysis,



determined by repeated sampling of an analytical NO tank ($\delta^{15}\text{N-NO} = -71.4\%$) under diverse collection conditions, is $\pm 1.1\%$ (Yu and Elliott, 2017).

3 Results

290 Sixty-three NO collection samples were obtained from the incubation experiments. The NO collection efficiency
calculated based on the measured $\text{NO}_2^- + \text{NO}_3^-$ concentration in the TEA solution and the theoretical concentration
based on the measured net NO production rate (Yu and Elliott, 2017) was on average $99.1 \pm 3.7\%$. Out of the sixty-
three collection samples, four samples had a NO collection efficiency lower than 95%. These samples were
excluded from further data analysis and interpretation. The measured N concentrations, net NO production rates, and
295 isotope data from all the incubation experiments are available in Table S5 to Table S11 in the Supplement.

3.1 Anoxic incubation

During the anoxic incubation, soil NO_3^- concentration decreased linearly from $49.3 \pm 0.1 \mu\text{g N}\cdot\text{g}^{-1}$ to $23.1 \pm 0.2 \mu\text{g N}\cdot\text{g}^{-1}$ (Fig. 2a), while NO_2^- concentration increased linearly from $0.4 \pm 0.1 \mu\text{g N}\cdot\text{g}^{-1}$ to $6.9 \pm 0.1 \mu\text{g N}\cdot\text{g}^{-1}$ (Fig. 2b). The
net NO production rate ($f_{\text{NO-anoxic}}$) increased progressively from the first sampling day ($72 \pm 8 \text{ ng N}\cdot\text{g}^{-1}\cdot\text{h}^{-1}$) to
300 sampling day 5 and then stabilized at about $82 \text{ ng N}\cdot\text{g}^{-1}\cdot\text{h}^{-1}$ (Fig. 2c).

$\delta^{15}\text{N-NO}_3^-$ and $\delta^{15}\text{N-NO}$ values increased from 4.7 ± 0.3 to $38.7 \pm 1.5\%$ and -44.7 ± 0.3 to $-22.8 \pm 2.2\%$,
respectively, over the anoxic incubation (Fig. 2d and 2f). The difference between $\delta^{15}\text{N-NO}_3^-$ and $\delta^{15}\text{N-NO}$ values
increased significantly from 49.4 to 59.5‰ toward the end of the incubation (Fig. 2d and 2f). Based on the closed-
system Rayleigh model, the apparent N isotopic fractionation during NO_3^- consumption was estimated to be
305 $43.3 \pm 0.9\%$ (Fig. S3 in the Supplement). $\delta^{15}\text{N-NO}_2^-$ was estimated for samples collected in the last three sampling
days where NO_2^- accounted for >15% of the $\text{NO}_3^- + \text{NO}_2^-$ pool. The estimated $\delta^{15}\text{N-NO}_2^-$ values were $-6.9 \pm 3.7\%$, $-$
 $6.0 \pm 2.5\%$, and $-0.9 \pm 1.3\%$, respectively (Fig. 2e). Although limited to the last three sampling days, $\delta^{15}\text{N-NO}_2^-$ was
lower than $\delta^{15}\text{N-NO}_3^-$ by 33.6 to 37.9‰ (Fig. 2d and 2e), but was higher than the concurrently measured $\delta^{15}\text{N-NO}$
values by a relatively constant offset of $21.5 \pm 0.7\%$ (Fig. 2e and 2f). Surprisingly, both $\delta^{18}\text{O-NO}_3^-$ values (33.4 ± 0.2
310 to $23.1 \pm 0.3\%$) and $\Delta^{17}\text{O-NO}_3^-$ values (10.0 ± 0.2 to $0.7 \pm 0.2\%$) decreased progressively over the course of the anoxic
incubation and were entirely decoupled from $\delta^{15}\text{N-NO}_3^-$ (Fig. 2g and 2h).

3.2 Oxic and hypoxic incubations

Over the oxic incubation, soil NH_4^+ concentration decreased linearly with increasing NO_3^- concentration under all
three $\delta^{15}\text{N-NH}_4^+$ treatments (Fig. 3a and 3b). In the hypoxic incubation, changes in NH_4^+ and NO_3^- concentrations
315 were more limited, although the linear trends were still evident (Fig. 3a and 3b). Under both oxic and hypoxic
conditions, the total concentration of soil NH_4^+ and NO_3^- remained nearly constant over the entire incubations (i.e.,
variations < 4%), and soil NO_2^- concentration was below the detection limit in both incubations. In the oxic
incubation, $\delta^{15}\text{N-NH}_4^+$ values uniformly increased by 8.6 to 13.1‰ under all three $\delta^{15}\text{N-NH}_4^+$ treatments (Fig. 3e),
while $\delta^{15}\text{N-NO}_3^-$ values varied distinctly, depending on the initial $\delta^{15}\text{N-NH}_4^+$ values (Fig. 3d). Specifically, $\delta^{15}\text{N-}$
320 NO_3^- values increased by 7.8‰ and decreased by 10.9‰ under the high and low $\delta^{15}\text{N-NH}_4^+$ treatments, respectively,



and remained relatively constant under the intermediate $\delta^{15}\text{N-NH}_4^+$ treatment (Fig. 3d). Limited increases in $\delta^{15}\text{N-NH}_4^+$ values ($<2\text{‰}$) were observed under all three $\delta^{15}\text{N-NH}_4^+$ treatments in the hypoxic incubation (Fig. 3e). Correspondingly, variations in $\delta^{15}\text{N-NO}_3^-$ values were much smaller in the hypoxic incubation compared to those revealed in the oxic incubation (Fig. 3d). In both oxic and hypoxic incubations, $\delta^{18}\text{O-NO}_3^-$ (Fig. 3g) and $\Delta^{17}\text{O-NO}_3^-$ (Fig. 3h) values decreased progressively under all three $\delta^{15}\text{N-NH}_4^+$ treatments, although the rates of decrease were significantly higher in the oxic incubation (Fig. 3g and 3h).

The net NO production was significantly higher in the hypoxic incubation ($f_{\text{NO-hypoxic}}$; 9.0 to 10.4 $\text{ng N}\cdot\text{g}^{-1}\cdot\text{h}^{-1}$) than in the oxic incubation ($f_{\text{NO-oxic}}$; 7.1 to 8.5 $\text{ng N}\cdot\text{g}^{-1}\cdot\text{h}^{-1}$) (Fig. 3c). The measured $\delta^{15}\text{N-NO}$ values ranged from -16.8 ± 0.3 to $-54.9\pm 0.8\text{‰}$ in the oxic incubation and from -21.3 ± 0.0 to $-51.4\pm 0.4\text{‰}$ in the hypoxic incubation (Fig. 3f). Pooling all the $\delta^{15}\text{N-NO}$ measurements, we found that $\delta^{15}\text{N}$ values between NH_4^+ and NO differed from 58.9 to 70.7‰ across the three $\delta^{15}\text{N-NH}_4^+$ treatments in the oxic incubation and from 50.4 to 69.6‰ in the hypoxic incubation (Fig. 4). In both incubations, the largest difference was observed under the high $\delta^{15}\text{N-NH}_4^+$ treatment, while the smallest difference was observed under the low $\delta^{15}\text{N-NH}_4^+$ treatment. Under both oxic and hypoxic conditions, there was a significant linear relationship between the measured $\delta^{15}\text{N-NO}$ and $\delta^{15}\text{N-NH}_4^+$ values from all three $\delta^{15}\text{N-NH}_4^+$ treatments (Fig. 4). The slope of the linear relationship is 0.78 ± 0.03 (± 1 SE) and 0.61 ± 0.05 for the oxic and hypoxic incubations, respectively (Fig. 4).

3.3 Abiotic NO production

Addition of NO_3^- or NH_4^+ to the sterilized soil did not result in detectable NO production under either oxic or anoxic condition. Immediate NO release was, however, triggered by NO_2^- addition under anoxic conditions (Fig. 5a). The abiotic NO production rate ($f_{\text{NO-abiotic}}$) reached a steady level of 83 ± 5 $\text{ng N}\cdot\text{g}^{-1}\cdot\text{h}^{-1}$ several minutes after the NO_2^- addition and then decreased exponentially to < 3 $\text{ng N}\cdot\text{g}^{-1}\cdot\text{h}^{-1}$ over the following 8 days (Fig. 5a). The natural logarithm of $f_{\text{NO-abiotic}}$ showed a linear relationship with time (Fig. 5b). The NO produced following the NO_2^- addition had a $\delta^{15}\text{N}$ value of $-17.8\pm 0.4\text{‰}$, giving rise to a $\delta^{15}\text{N}$ offset between NO_2^- and NO of $19.2\pm 0.5\text{‰}$.

4 Discussion

Because interpretations of the results from the incubation experiments build upon each other, here we discuss the results from incubation of the sterilized soils (hereafter, abiotic incubation), anoxic incubation, and oxic/hypoxic incubations successively.

4.1 Reaction characteristics and N isotopic fractionation during abiotic NO production

The immediate release of NO upon the addition of NO_2^- highlights the chemically unstable nature of NO_2^- and the critical role of chemical NO_2^- reactions in driving soil NO emissions (Venterea et al., 2005; Lim et al., 2018). The strong linearity between $\ln(f_{\text{NO-abiotic}})$ and time (Fig. 5b) suggests apparent first-order kinetics for the abiotic NO production from NO_2^- (Equations 2 and 3) (McKenney et al., 1990).

$$f_{\text{NO-abiotic}} = s_{\text{abiotic}} \times k_{\text{abiotic}} \times [\text{NO}_2^-]_t \quad \text{Equation (2)}$$

$$[\text{NO}_2^-]_t = [\text{NO}_2^-]_0 e^{-k_{\text{abiotic}} \times t} \quad \text{Equation (3)}$$



355 In Equations 2 and 3, t is time; k_{abiotic} is the pseudo-first order rate constant for NO_2^- loss; s_{abiotic} is the apparent stoichiometric coefficient for NO production from NO_2^- ; and $[\text{NO}_2^-]_t$ and $[\text{NO}_2^-]_0$ are NO_2^- concentration at time t and $t=0$ in the sterilized soil, respectively. Combining Equations 2 and 3 and then log-transforming both sides yield:

$$\ln(f_{\text{NO-abiotic}}) = -k_{\text{abiotic}} \times t + \ln(s_{\text{abiotic}} \times k_{\text{abiotic}} \times [\text{NO}_2^-]_0) \quad \text{Equation (4)}$$

360 According to Equation 4, k_{abiotic} and s_{abiotic} are estimated using the slope and intercept of the linear regression of $\ln(f_{\text{NO-abiotic}})$ versus time (Fig. 5b). Given $[\text{NO}_2^-]_0 = 8 \mu\text{g N} \cdot \text{g}^{-1}$, s_{abiotic} and k_{abiotic} are estimated to be 0.52 ± 0.05 ($\pm\text{SE}$) and $0.019 \pm 0.002 \text{ h}^{-1}$, respectively, suggesting that NO accounted for $52 \pm 5\%$ of the reacted NO_2^- during the abiotic incubation. The estimated k_{abiotic} is within the range (i.e., 0.00055 to 0.73 h^{-1}) derived by a recent study based on soil samples spanning a wide range of pH values (3.4 to 7.2) (Lim et al., 2018). Based on the estimated k_{abiotic} , 97% of the added NO_2^- was lost by the end of the abiotic incubation.

365 Several reaction pathways with distinct stoichiometry have been proposed for abiotic NO production from NO_2^- in soils. Under acidic soil conditions, self-decomposition of HNO_2 produces NO and nitric acid (HNO_3) with a stoichiometric HNO_2 -to-NO ratio ranging from 0.5 to 0.66 (i.e., 1 mole of HNO_2 produces 0.5 to 0.66 mole of NO) (Van Cleemput and Samater, 1995). Although at pH 5.7, HNO_2 constituted $<1\%$ of the $\text{NO}_2^- + \text{HNO}_2$ pool in this soil, HNO_2 decomposition can occur on acidic clay mineral surfaces, even though bulk soil pH is circumneutral
370 (Venterea et al., 2005). However, given the complete NO_2^- consumption in the abiotic incubation, HNO_2 decomposition confined to acidic microsites could not account for all observed NO production. Under anoxic conditions, $\text{NO}_2^-/\text{HNO}_2$ can also be stoichiometrically reduced to NO by transition metals (e.g., Fe(II)) and diverse organic molecules (e.g., humic and fulvic acids, lignins, and phenols) in a process termed chemo-denitrification (Zhu-Baker et al., 2015). The produced NO from chemo-denitrification can undergo further reduction to form N_2O
375 and N_2 (Zhu-Baker et al., 2015). In addition, both NO_2^- and NO in soil solution can be consumed as nitroso donors in abiotic nitrosation reactions, resulting in N incorporation into soil organic matter (Heil et al., 2016; Lim et al., 2018). Therefore, our observation that about half of the reacted NO_2^- was recovered as NO may result from multiple competing NO_2^- sinks, parallel NO-producing pathways, and possibly abiotic NO consumption in the sterilized soil. The other half of the reacted NO_2^- that could not be accounted for by the measured NO was likely present in the
380 forms of N_2O , N_2 , and/or nitrosated organic compounds in the soil.

The observed $\delta^{15}\text{N}$ difference between NO_2^- and NO (i.e., $^{15}\eta_{\text{NO}_2/\text{NO}(\text{abiotic})} = 19.2 \pm 0.5\%$) likely reflects a combined N isotope effect for all of the competing NO production pathways during the abiotic incubation. While very little isotope data exist for abiotic NO_2^- reactions in the literature, the measured $^{15}\eta_{\text{NO}_2/\text{NO}(\text{abiotic})}$ in this study is consistent with reported N isotope effects (i.e., 15 to 25%) for abiotic NO_2^- reduction by Fe(II) at similar NO_2^-
385 consumption rates as this study (0.02 to 0.05 h^{-1}) (Buchwald et al., 2016). On the other hand, the measured $^{15}\eta_{\text{NO}_2/\text{NO}(\text{abiotic})}$ is lower than the reported $\delta^{15}\text{N}$ offsets between NO_2^- and N_2O (i.e., $^{15}\eta_{\text{NO}_2/\text{N}_2\text{O}(\text{abiotic})}$) for chemo-denitrification (24 to 29%) (Jones et al., 2015; Wei et al., 2019). This seems to suggest that the observed abiotic NO production was mainly driven by chemo-denitrification and that accumulation of NO as an chemo-denitrification intermediate may explain why the observed $^{15}\eta_{\text{NO}_2/\text{N}_2\text{O}(\text{abiotic})}$ was larger than the N isotope effect for Fe(II)-catalyzed
390 NO_2^- reduction in previous batch experiments (Jones et al., 2015; Buchwald et al., 2016). Future studies adopting



simultaneous $\delta^{15}\text{N-NO}$ and $\delta^{15}\text{N-N}_2\text{O}$ measurements will be required to elucidate the role of NO as the N_2O precursor during chemo-denitrification.

It is important to note that the autoclaving is a harsh sterilization method and can substantially alter soil physical and chemical properties. For example, Buessecker et al. (2019) recently showed that autoclaved peat soil had 10-fold higher total fluorescence compared to non-sterilized controls, indicating dramatic increases in solubility and lability of organic molecules by autoclaving. Furthermore, autoclaving has also been shown to substantially increase abiotic N_2O production from NO_2^- -amended soils (Wei et al., 2019). Conversely, milder sterilization methods (e.g., gamma-irradiation) that presumably cause less alteration of soil properties may not completely inactivate biological NO production due to the high diversity of biological NO production pathways in soils (e.g., non-specific reactions catalyzed by extracellular enzymes) (Medinets et al., 2015). Further research is warranted to compare different sterilization methods for their effects on abiotic NO production and $^{15}\eta_{\text{NO}_2/\text{NO}(\text{abiotic})}$.

4.2 Reaction reversibility between NO_3^- and NO_2^- and N isotope distribution between NO_3^- , NO_2^- , and NO during the anoxic incubation

The measured $f_{\text{NO-anoxic}}$ (72 to 82 $\text{ng N}\cdot\text{g}^{-1}\cdot\text{h}^{-1}$) (Fig. 2c) is well within the range reported for anoxic soil incubations (e.g., 5 to 500 $\text{ng N}\cdot\text{g}^{-1}\cdot\text{h}^{-1}$) (Medinets et al., 2015), and is about 2/3 of the net consumption rate of $\text{NO}_3^- + \text{NO}_2^-$ during the anoxic incubation. That the majority of consumed $\text{NO}_3^- + \text{NO}_2^-$ was recovered as NO supports the emerging notion that NO can be the end product of denitrification once limitations on gas diffusion are lifted in soils (Russow et al., 2009; Loick et al., 2016). Applying the derived k_{abiotic} and s_{abiotic} in the abiotic incubation to the measured NO_2^- concentrations under anoxic condition produced a range of $f_{\text{NO-abiotic}}$ from < 4 to 68 $\text{ng N}\cdot\text{g}^{-1}\cdot\text{h}^{-1}$ (Fig. S4 in the Supplement). While this modeled $f_{\text{NO-abiotic}}$ appears to contribute up to 80% of the measured $f_{\text{NO-anoxic}}$ (Fig. S4 in the Supplement), $f_{\text{NO-anoxic}}$ was high and remained stable even without any significant accumulation of NO_2^- in the soil (Fig. 2b and 2c), suggesting that k_{abiotic} was likely overestimated in the abiotic incubation (see above). Assuming that net biological NO production was maintained at the level of $f_{\text{NO-anoxic}}$ measured during the first sampling event and that s_{abiotic} was constant and equal to 0.52, a back-of-the-envelope calculation based on the difference in $f_{\text{NO-anoxic}}$ between the first and last sampling events and the NO_2^- concentration measured at the end of the anoxic incubation indicates that k_{abiotic} was likely on the order of 0.0027 h^{-1} , or about 7 times lower than the k_{abiotic} derived in the abiotic incubation. Although qualitative, this calculation suggests a minor contribution of abiotic NO production to the measured $f_{\text{NO-anoxic}}$ (<12%; Fig. S4 in the Supplement).

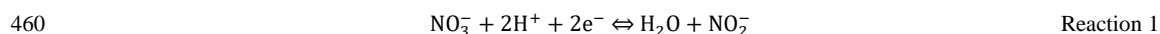
The large increases in $\delta^{15}\text{N-NO}_3^-$ and $\delta^{15}\text{N-NO}$ values over the anoxic incubation (Fig. 2d and 2f) are congruent with strong N isotopic fractionations during microbial denitrification (Mariotti et al., 1981; Granger et al., 2008). However, the observed net isotope effect for NO production from NO_3^- (i.e., $^{15}\eta_{\text{NO}_3/\text{NO}}$; 49.4 to 59.5‰) is larger than the apparent N isotope effect for NO_3^- consumption ($43.3 \pm 0.9\%$) (Fig. S3 in the Supplement). The large magnitude and increasing pattern of $^{15}\eta_{\text{NO}_3/\text{NO}}$, together with the accumulation of NO_2^- in the soil, point to complexity beyond single-step isotopic fractionations and highlight the need to carefully examine fractionation mechanisms for all intermediate steps leading to net NO production (i.e., NO_3^- to NO_2^- , NO_2^- to NO, and NO to N_2O). Moreover, it is surprising that both $\delta^{18}\text{O-NO}_3^-$ and $\Delta^{17}\text{O-NO}_3^-$ values decreased over the anoxic incubation (Fig. 2g and 2h). Interestingly, similar decreasing trends in $\delta^{18}\text{O-NO}_3^-$ values (e.g., up to 4‰ over 25 h) have been



reported by Lewicka-Szczepak et al. (2014) for two anoxically incubated agricultural soils amended with a high- $\delta^{18}\text{O}$ Chilean NO_3^- fertilizer similar to ours (i.e., $\delta^{18}\text{O}\text{-NO}_3^- = 56\%$), although $\Delta^{17}\text{O}\text{-NO}_3^-$ was not reported in this
430 previous study. The decreasing $\delta^{18}\text{O}\text{-NO}_3^-$ values, observed here and by Lewicka-Szczepak et al. (2014), appear to contradict the well-established paradigm that variations in $\delta^{15}\text{N}\text{-NO}_3^-$ and $\delta^{18}\text{O}\text{-NO}_3^-$ values follow a linear trajectory with a slope of 0.5 to 1 during dissimilatory NO_3^- reduction (Granger et al., 2008). Furthermore, as $\Delta^{17}\text{O}\text{-NO}_3^-$ is in theory not altered by microbial denitrification – a mass-dependent fractionation process (Michalski et al., 2004; Yu and Elliott, 2018), the decreasing $\Delta^{17}\text{O}\text{-NO}_3^-$ values observed in this study indicate that processes capable of diluting
435 or erasing the $\Delta^{17}\text{O}$ signal may occur concurrently with denitrification during the anoxic incubation. Importantly, if this dilution or removal of the $\Delta^{17}\text{O}$ signal was accompanied by N isotopic fractionations, there may be cascading effects on the distribution of N isotopes between NO_3^- , NO_2^- , and NO .

The decreasing $\delta^{18}\text{O}\text{-NO}_3^-$ and $\Delta^{17}\text{O}\text{-NO}_3^-$ values could be potentially explained by an O isotope equilibration between NO_3^- and soil H_2O , catalyzed either chemically or biologically via a reversible reaction
440 between NO_3^- and NO_2^- (Granger and Wankel, 2016). However, it has been shown in controlled laboratory experiments that dissimilatory NO_3^- reduction catalyzed by bacterial nitrate reductase (NAR) is irreversible at the enzyme level (Treiber and Granger, 2017) and that abiotic O isotope exchange between NO_3^- and H_2O is extremely slow (half-life $>10^9$ y at 25°C and pH 7) and therefore irrelevant under natural soil conditions (Kaneko and Poulson, 2013). Although fungi use a distinct enzyme system for denitrification (Shoun et al., 2012), there is no
445 evidence for enzymatic reversibility of fungal NAR in the literature. Furthermore, by converting NH_4^+ and NO_2^- simultaneously to N_2 and NO_3^- , anaerobic NH_4^+ oxidation (anammox) could dilute the $\Delta^{17}\text{O}$ signal by producing NO_3^- with $\Delta^{17}\text{O}=0$ (Brunner et al., 2013). However, due to the low indigenous NH_4^+ concentration, anammox is considered not pertinent during the anoxic incubation. Given the complete recovery of NO_3^- concentrations and isotopes in the control experiments (Table S1 and Table S2 in the Supplement), as well as the significantly increased
450 $\delta^{15}\text{N}\text{-NO}_3^-$ values during the anoxic incubation, we excluded NO_3^- production from aerobic NH_4^+ oxidation as a possible explanation for the observed declines in $\delta^{18}\text{O}\text{-NO}_3^-$ and $\Delta^{17}\text{O}\text{-NO}_3^-$ values.

Therefore, having ruled out the above possibilities led us to postulate that the decreasing $\delta^{18}\text{O}\text{-NO}_3^-$ and $\Delta^{17}\text{O}\text{-NO}_3^-$ values may result from anaerobic NO_2^- oxidation mediated by NOB in the soil. The enzyme catalyzing
455 NO_2^- oxidation to NO_3^- in NOB – NO_2^- oxidoreductase (NXR) – is metabolically versatile and has been shown to catalyze NO_3^- reduction under anoxic conditions by operating in reverse (Friedman et al., 1986; Freitag et al., 1987; Bock et al., 1988; Koch et al., 2015). Moreover, during NXR-catalyzed NO_2^- oxidation, the required O atom originates from H_2O molecules (Reaction 1), so that NO_2^- can in theory be oxidized to NO_3^- without the presence of O_2 by donating electrons to redox-active intracellular components (Wunderlich et al., 2013) or alternative electron acceptors in niche environments (Babbin et al., 2017).

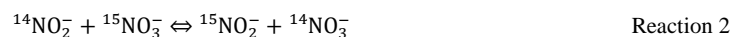


In a denitrifying environment, anaerobic oxidation of denitrification-produced NO_2^- back to NO_3^- (i.e., NO_2^- re-oxidation) can dilute $\delta^{18}\text{O}\text{-NO}_3^-$ and $\Delta^{17}\text{O}\text{-NO}_3^-$ values by incorporating a ‘new’ O atom from H_2O into the reacting NO_3^- pool (Reaction 1) (Granger and Wankel, 2016). Under acidic and circumneutral pH conditions, this dilution effect can be further enhanced by chemically- and perhaps biologically-catalyzed O isotope equilibration between



465 NO_2^- and H_2O (Casciotti et al., 2007; Buchwald and Casciotti, 2010), which effectively erase the isotopic imprints of
denitrification on NO_2^- prior to its re-oxidation. The reversibility of NXR and its direct control on O isotopes in NO_3^-
have been convincingly demonstrated by Wunderlich et al. (2013) using a pure culture of *Nitrobacter vulgaris*. By
incubating *N. vulgaris* in a NO_3^- solution under anoxic conditions, Wunderlich et al. (2013) showed that NO_2^- was
470 produced in the solution by *N. vulgaris* and that *N. vulgaris* promoted incorporation of amended ^{18}O - H_2O labels into
 NO_3^- through a re-oxidation of the accumulated NO_2^- (Wunderlich et al., 2013).

Importantly, there is mounting evidence from the marine N cycle community that NO_2^- re-oxidation plays a
critical role in the N isotope partitioning between NO_3^- and NO_2^- . At the process scale, NO_2^- re-oxidation co-
occurring with dissimilatory NO_3^- reduction can lead to a large $\delta^{15}\text{N}$ difference between NO_3^- and NO_2^- beyond what
would be expected to result from NO_3^- reduction alone (Gaye et al., 2013; Dale et al., 2014; Dähnke and Thamdrup,
475 2015; Peters et al., 2016; Martin and Casciotti, 2017; Buchwald et al., 2018). This large $\delta^{15}\text{N}$ difference is thought to
arise from a rare, but intrinsic, inverse kinetic isotope effect associated with NO_2^- re-oxidation (e.g., -13‰)
(Casciotti et al., 2009). As such, in a net denitrifying environment, NO_2^- re-oxidation functions as an apparent
branching pathway along the sequential reduction of NO_3^- , preferentially re-oxidizing $^{15}\text{NO}_2^-$ back to NO_3^- . At the
enzyme scale, the bidirectional NXR enzyme has been proposed to catalyze intracellular coupled NO_3^- reduction and
480 NO_2^- oxidation (i.e., bidirectional interconversion of NO_3^- and NO_2^-), facilitating expression of an equilibrium N
isotope effect between NO_3^- and NO_2^- (Reaction 2) (Wunderlich et al., 2013; Kemeny et al., 2016).



Evidence from pure culture studies of anammox bacteria carrying the NXR enzyme (Brunner et al., 2013) and
theoretical quantum calculations (Casciotti, 2009) suggests that this N isotope equilibration favors partitioning of
485 ^{14}N into NO_2^- with an equilibrium isotope effect ranging from -50 to -60‰ (negative sign is used to denote that this
N isotope equilibration partitions ^{14}N to the left side of Reaction 2). This NXR-catalyzed $\text{NO}_3^-/\text{NO}_2^-$ interconversion
was invoked to explain the extremely low $\delta^{15}\text{N}$ - NO_2^- values relative to $\delta^{15}\text{N}$ - NO_3^- (up to 90‰) in the surface
Antarctic ocean, where aerobic NO_2^- oxidation is inhibited by low nutrient availability (Kemeny et al., 2016).
Hypothetically, if expressed at either the process or the enzyme level, the N isotope effect for NO_2^- re-oxidation
490 could propagate into denitrification-produced NO , giving rise to an increased $\delta^{15}\text{N}$ difference between NO_3^- and NO
($^{15}\eta_{\text{NO}_3/\text{NO}}$).

To test whether NO_2^- re-oxidation can explain the observed declines in $\delta^{18}\text{O}$ - NO_3^- and $\Delta^{17}\text{O}$ - NO_3^- values
and $\delta^{15}\text{N}$ distribution between NO_3^- , NO_2^- , and NO , we modified an isotopologue-specific (i.e., ^{14}N , ^{15}N , ^{16}O , ^{17}O ,
and ^{18}O) numerical model previously described by Yu and Elliott (2018) to simulate co-occurring denitrification and
495 NO_2^- re-oxidation in two steps. Without a clear identification of the alternative electron acceptors that coupled with
anaerobic NO_2^- oxidation in the studied soil, we followed the reaction scheme proposed by Wunderlich et al. (2013)
and Kemeny et al. (2016) (Reaction 1) to parameterize the NXR-catalyzed NO_2^- re-oxidation as the backward
reaction of a dynamic equilibrium between NO_3^- and NO_2^- (Fig. 6) – that is, the NXR-catalyzed NO_2^- re-oxidation
(backward reaction) is balanced by an NXR-catalyzed NO_3^- reduction (forward reaction), leading to no net NO_2^-
500 oxidation or NO_3^- reduction in the soil. Importantly, this representation is consistent with the observation that both
 NO_3^- consumption and NO_2^- accumulation followed a pseudo-zero order kinetics over the anoxic incubation (Fig. 2a



and 2b), which implies no net contribution from the $\text{NO}_3^-/\text{NO}_2^-$ interconversion. Given previous findings that the NXR-catalyzed O exchange between NO_3^- and NO_2^- depends on NO_2^- availability (Wunderlich et al., 2013), the backward NO_2^- re-oxidation was assumed to be first order (with respect to NO_2^-), defined by a first order rate constant, $k_{\text{NXR}(b)}$. With respect to the O isotope equilibration between H_2O and the reacting NO_2^- pool, we considered two extreme case scenarios: (1) no exchange and (2) complete exchange. In the “no exchange” scenario, the imprints of denitrification on $\delta^{18}\text{O}-\text{NO}_2^-$ and $\Delta^{17}\text{O}-\text{NO}_2^-$ values are preserved, such that only one H_2O -derived O atom is incorporated into NO_3^- with each NO_2^- molecule being re-oxidized (Reaction 1). In the “complete exchange” scenario, $\delta^{18}\text{O}$ and $\Delta^{17}\text{O}$ values of NO_2^- always reflect those of soil H_2O ($\delta^{18}\text{O}-\text{H}_2\text{O}\approx -10\text{‰}$, $\Delta^{17}\text{O}-\text{H}_2\text{O}=0\text{‰}$) (Fig. 6), and therefore all three O atoms in NO_3^- produced from NO_2^- re-oxidation originate from H_2O . Furthermore, we considered both abiotic NO production and denitrification as the source of NO during the anoxic incubation (Fig. 6). To account for the potential overestimation in k_{abiotic} (see above), we used a reduced k_{abiotic} (0.0027 h^{-1}) to model abiotic NO production from NO_2^- , while s_{abiotic} and $^{15}\eta_{\text{NO}_2/\text{NO}(\text{abiotic})}$ were fixed at 0.52 and 19.2‰, respectively. With respect to $\delta^{15}\text{N}$ of denitrification-produced NO, we assumed that NIR-catalyzed NO_2^- reduction to NO and NOR-catalyzed NO reduction to N_2O were each associated with a kinetic N isotope effect ($^{15}\eta_{\text{NIR}}$ and $^{15}\eta_{\text{NOR}}$). The closed-system Rayleigh equation was then used to simulate the coupled NO production and reduction in denitrification at each model time interval (Lewicka-Szczebak et al. 2014). Detailed model derivation and formulation are provided in the Supplement (Text S3.1).

With this model of co-occurring denitrification and NO_2^- re-oxidation, we first solved for the rates of denitrifier-catalyzed NO_3^- (R_{NAR}), NO_2^- (R_{NIR}), and NO (R_{NOR}) reductions and $k_{\text{NXR}(b)}$ (4 unknowns) using the measured NO_3^- and NO_2^- concentrations, $f_{\text{NO-anoxic}}$, and $\Delta^{17}\text{O}-\text{NO}_3^-$ values (4 measured variables). This first modeling step was robustly constrained by the measured $\Delta^{17}\text{O}-\text{NO}_3^-$, which essentially functions as a $^{15}\text{NO}_3^-$ tracer (Yu and Elliott, 2018) and is therefore particularly sensitive to NO_2^- re-oxidation. In the second modeling step, the measured $\delta^{15}\text{N}-\text{NO}_3^-$, $\delta^{15}\text{N}-\text{NO}_2^-$, and $\delta^{15}\text{N}-\text{NO}$ values (3 measured variables) were used to optimize the kinetic N isotope effects for NAR-catalyzed NO_3^- reduction ($^{15}\eta_{\text{NAR}}$), $^{15}\eta_{\text{NIR}}$, $^{15}\eta_{\text{NOR}}$, and the equilibrium N isotope effect for NXR-catalyzed $\text{NO}_3^-/\text{NO}_2^-$ interconversion ($^{15}\eta_{\text{NXR}(eq)}$) (Reaction 2; Fig. 6) (4 unknowns). This modeling system is underdetermined (number of measured variables < number of unknowns) and thus cannot be solved uniquely. Thus, instead of definitively solving for the four unknown isotope effects, we explored their best combination to fit the measured $\delta^{15}\text{N}$ values of NO_3^- , NO_2^- , and NO. Specifically, to reduce the number of unknowns for model optimization, $^{15}\eta_{\text{NAR}}$ and $^{15}\eta_{\text{NXR}(eq)}$ were treated as known values, and $^{15}\eta_{\text{NIR}}$ and $^{15}\eta_{\text{NOR}}$ were solved by mapping through the entire space of $^{15}\eta_{\text{NAR}}$ and $^{15}\eta_{\text{NXR}(eq)}$ (at a resolution of 1‰), defined by their respective widest range of possible values. We used a range of 5 to 55‰ for $^{15}\eta_{\text{NAR}}$, consistent with a recent compilation based on soil incubations and denitrifier pure cultures (Denk et al., 2017). Given the existing observational and theoretical constraints (Casciotti, 2009; Brunner et al., 2013), a range of -60 to 0‰ was assigned to $^{15}\eta_{\text{NXR}(eq)}$, which is equivalent to the argument that the impact of $\text{NO}_3^-/\text{NO}_2^-$ interconversion on the N isotope distribution between NO_3^- and NO_2^- can vary from null to a strong partitioning of ^{14}N to NO_2^- . We further defined the lower 2.5th percentile of the error-weighted residual sum of squares (RSS) between simulated and measured $\delta^{15}\text{N}$ values of NO_3^- , NO_2^- , and



NO as the threshold for selection of the best-fit models. Detailed information regarding model optimization can be found in the Supplement (Text S3.2).

540 Results from the first modeling step are summarized in Table 1 and the best-fit models were plotted in Fig. 2 to compare with the measured data. Because the NXR-catalyzed $\text{NO}_3^-/\text{NO}_2^-$ interconversion was assumed to result in no change in NO_3^- and NO_2^- concentrations, R_{NAR} ($0.158 \mu\text{g N}\cdot\text{g}^{-1}\cdot\text{h}^{-1}$), R_{NIR} ($0.112 \mu\text{g N}\cdot\text{g}^{-1}\cdot\text{h}^{-1}$), and R_{NOR} ($0.039 \mu\text{g N}\cdot\text{g}^{-1}\cdot\text{h}^{-1}$) can be well-described by zero-order kinetics and are not sensitive to model scenarios for O exchange between NO_2^- and H_2O (Table 1). Moreover, the observed NO_2^- accumulation and $f_{\text{NO-anoxic}}$ dynamics can be well-
545 reproduced using the modeled denitrification rates and the downward adjustment of k_{abiotic} (Fig. 2b and 2c). $k_{\text{NXR(b)}}$ was estimated to be 0.64 h^{-1} and 0.25 h^{-1} under the “no exchange” and “complete exchange” scenarios, respectively (Table 1). Under both scenarios, the simulated $\Delta^{17}\text{O-NO}_3^-$ values exhibit a characteristic decreasing trend and are in excellent agreement with measured $\Delta^{17}\text{O-NO}_3^-$ values (Fig. 2h). The larger $k_{\text{NXR(b)}}$ under the “no exchange” scenario is expected and can be explained by the faster back reaction (i.e., NO_2^- re-oxidation) required to reproduce the
550 observed dilution of $\Delta^{17}\text{O-NO}_3^-$, because only one “new” O atom is incorporated into NO_3^- with each NO_2^- molecule being re-oxidized. Although the measured $\delta^{18}\text{O-NO}_3^-$ values did not provide quantitative constraints for the model optimization, the isotopologue-specific model with the optimized denitrification rates and $k_{\text{NXR(b)}}$ was run forward to test whether the decreasing $\delta^{18}\text{O-NO}_3^-$ values can also be possibly explained by co-occurring denitrification and NO_2^- re-oxidation (details are provided in Text S4 in the Supplement). The results showed that NO_3^- reduction
555 (acting to increase $\delta^{18}\text{O-NO}_3^-$ values) and NO_2^- re-oxidation (acting to decrease $\delta^{18}\text{O-NO}_3^-$ values) have counteracting effects on the forward-modeled $\delta^{18}\text{O-NO}_3^-$ (Fig. S2 in the Supplement) and that the decreasing trend in $\delta^{18}\text{O-NO}_3^-$ values can be well-reproduced under both “no exchange” and “complete exchange” scenarios with a reasonable assumption on the net O isotope effects for denitrification and NO_2^- re-oxidation (Fig. S2; see Text S4 in the Supplement) (Granger and Wankel, 2016). Therefore, although $k_{\text{NXR(b)}}$ cannot be definitively quantified in this
560 study due to the unknown degree of O exchange between NO_2^- and H_2O , these simulation results provide confidence in our hypothesis that the observed decreases in $\delta^{18}\text{O-NO}_3^-$ and $\Delta^{17}\text{O-NO}_3^-$ values were driven by the reversible action of the NXR enzyme. It is important to note that the estimated $k_{\text{NXR(b)}}$ is fairly large even under the “complete exchange” scenario. Based on the NO_2^- concentration measured at the end of the anoxic incubation ($6.9 \mu\text{g N}\cdot\text{g}^{-1}$), a $k_{\text{NXR(b)}}$ of 0.25 h^{-1} would require a NO_2^- re-oxidation rate ($1.7 \mu\text{g N}\cdot\text{g}^{-1}\cdot\text{h}^{-1}$) that is one order of magnitude higher
565 than the estimated R_{NAR} and R_{NIR} . However, the inferred maximum NO_2^- re-oxidation rate under either model scenario (1.7 to $4.4 \mu\text{g N}\cdot\text{g}^{-1}\cdot\text{h}^{-1}$) is still within the reported range for aerobic NO_2^- oxidation in agricultural soils (e.g., up to $6\text{--}7 \mu\text{g N}\cdot\text{g}^{-1}\cdot\text{h}^{-1}$) (Taylor et al., 2019), indicative of high NOB activity even under anoxic conditions (Koch et al., 2015).

570 Based on the modeled denitrification rates and $k_{\text{NXR(b)}}$, the best-fit $^{15}\eta_{\text{NXR(b)}}$ was confined to a narrow range from -40 to -35‰ (Fig. 7a and 7b) and was not sensitive to model scenarios for O equilibration between NO_2^- and H_2O (Fig. 8b). While the best-fit $^{15}\eta_{\text{NAR}}$ and $^{15}\eta_{\text{NXR(b)}}$ were positively correlated, especially under the “complete exchange” scenario (Fig. 7a and 7b), the best-fit $^{15}\eta_{\text{NAR}}$ spanned a wide range (5 to 45‰) and was significantly lower under the “no exchange” scenario (RSS-weighted mean: 19‰) relative to the “complete exchange” scenario (RSS-weighted mean: 30‰) (Fig. 8a). On the other hand, the best-fit $^{15}\eta_{\text{NIR}}$ (15 to 22‰) and $^{15}\eta_{\text{NOR}}$ (-8 to 2‰) did



575 not vary substantially and were similar between the two model scenarios (Fig. 7c to 7d; Fig. 8c and 8d). Under both
model scenarios, the measured $\delta^{15}\text{N-NO}_3^-$, $\delta^{15}\text{N-NO}_2^-$, and $\delta^{15}\text{N-NO}$ values can be well-simulated using the RSS-
weighted mean $^{15}\eta$ values from the best-fit models (Fig. 2d to 2f). Specifically, the modeled difference between
 $\delta^{15}\text{N-NO}_3^-$ and $\delta^{15}\text{N-NO}_2^-$ values increased from about 29‰ at the beginning of the incubation to about 38‰ at the
580 end of the incubation (Fig. 2d and 2e), whereas a constant $\delta^{15}\text{N}$ offset of about 20‰ was revealed between the
modeled $\delta^{15}\text{N-NO}_2^-$ and $\delta^{15}\text{N-NO}$ values (Fig. 2e and 2f). Therefore, the modeled $^{15}\eta$ values and $\delta^{15}\text{N-NO}_2^-$
dynamics reveal important new information for understanding the increasing $^{15}\eta_{\text{NO}_3^-/\text{NO}_2^-}$ over the anoxic incubation.
During the early phase of the incubation, the N isotope partitioning between NO_3^- , NO_2^- , and NO was mainly
controlled by denitrification and its associated isotope effects (i.e., $^{15}\eta_{\text{NAR}}$, $^{15}\eta_{\text{NIR}}$, and $^{15}\eta_{\text{NOR}}$). With the increasing
accumulation of NO_2^- in the soil, the dominant control on the $\delta^{15}\text{N}$ distribution shifted to the N isotope exchange
585 between NO_3^- and NO_2^- , so that the difference between the $\delta^{15}\text{N-NO}_3^-$ and $\delta^{15}\text{N-NO}_2^-$ values was primarily
determined by $^{15}\eta_{\text{NXR}(\text{eq})}$ (-40 to -35‰). The revealed positive correlation between the best-fit $^{15}\eta_{\text{NAR}}$ and $^{15}\eta_{\text{NXR}(\text{b})}$
(Fig. 7a and 7b) and the significantly lower $^{15}\eta_{\text{NAR}}$ under the “no exchange” scenario (Fig. 8a) essentially reflect a
trade-off between $^{15}\eta_{\text{NAR}}$ and $^{15}\eta_{\text{NXR}(\text{b})}$ in controlling the $\delta^{15}\text{N}$ difference between NO_3^- and NO_2^- – that is, when the
interconversion between NO_3^- and NO_2^- is fast and the magnitude of $^{15}\eta_{\text{NXR}(\text{eq})}$ is large (i.e., very negative), only a
590 small $^{15}\eta_{\text{NAR}}$ is required to sustain the large $\delta^{15}\text{N}$ difference between NO_3^- and NO_2^- over the course of the anoxic
incubation.

The estimated $^{15}\eta_{\text{NXR}(\text{eq})}$ from the best-fit models is higher (i.e., closer to zero) than those derived from
theoretical calculations and pure culture studies (-50 to -60‰) (Casciotti, 2009; Brunner et al., 2013). Given the
heterogeneous distribution of substrates in soils, the lower absolute magnitude of the best-fit $^{15}\eta_{\text{NXR}(\text{eq})}$ may be due to
595 the partial rate limitation by transport of $\text{NO}_2^-/\text{NO}_3^-$ to the active site of NXR. As such, the best-fit $^{15}\eta_{\text{NXR}(\text{eq})}$ should
provide a conservative estimate of the intrinsic equilibrium isotope effect. Thus, the results from the anoxic
incubation underscore the important, yet previously unrecognized, role of the reversible $\text{NO}_3^-/\text{NO}_2^-$ interconversion
in controlling the $\delta^{15}\text{N}$ dynamics of soil NO_3^- and its denitrification products. Substantial re-oxidation of NO_2^- under
anoxic conditions seems paradoxical, but is underpinned by the increasingly recognized high degree of metabolic
600 versatility of NOB, including simultaneous oxidation of an organic substrate and NO_2^- , as well as parallel use of
 NO_3^- and O_2 as electron acceptors (Koch et al., 2015). In the absence of O_2 , few electron acceptors exist at common
environmental pH that have a higher redox potential than the $\text{NO}_3^-/\text{NO}_2^-$ pair (Wunderlich et al., 2013; Babbín et al.,
2017). It is therefore likely that NOB would gain energy by performing the intracellular coupled oxidation of NO_2^-
and reduction of NO_3^- to survive periods of O_2 deprivation. Although anaerobic NO_2^- oxidation until now has been
605 conclusively shown only in anoxic ocean water columns (Sun et al., 2017; Babbín et al., 2017) and aquatic
sediments (Wunderlich et al., 2013), soils host a huge diversity of coexisting NOB (Le Roux et al., 2016) and the
physiological flexibility of NOB beyond aerobic NO_2^- oxidation may contribute to the unexpected higher
abundances and activities of NOB relative to AOB and AOA in agricultural soils (Høberg et al., 1996; Ke et al.,
2013). Using the modified isotopologue-specific model, we demonstrate the possibility that large $^{15}\eta_{\text{NAR}}$ can be an
610 artifact of an isotopic equilibrium between NO_3^- and NO_2^- , occurring in connection with the bifunctional NXR
enzyme. Therefore, effective expressions of $^{15}\eta_{\text{NXR}(\text{eq})}$ in concurrence with $^{15}\eta_{\text{NAR}}$ may explain why $^{15}\eta_{\text{NAR}}$ estimated



615 by some anoxic soil incubations (e.g., 25 to 65‰) are far larger than those reported by studies of denitrifying and
NO₃⁻-reducing bacterial cultures (e.g., 5 to 30‰) (Denk et al., 2017) and why the slope of δ¹⁸O-NO₃⁻ versus δ¹⁵N-
NO₃⁻ values during denitrification in many field studies was not constant and rarely close to unity as observed in
pure denitrifying cultures (Granger and Wankely, 2016). Indeed, evidence for a reversible enzymatic pathway
linking NO₃⁻ and NO₂⁻ under anoxic conditions has already been documented in previous soil studies (e.g., Kool et
al., 2011; Lewicka-Szczebak et al., 2014), implying its wide occurrence in soils. More studies using soils from a
broad range of environments are needed to pinpoint the exact mechanisms by which NO₂⁻ can be anaerobically
oxidized in soils. To that end, Δ¹⁷O-NO₃⁻ can be used as a powerful benchmark for disentangling co-occurring NO₃⁻
620 reduction and NO₂⁻ re-oxidation.

The best-fit ¹⁵η_{NIR} (15 to 22‰) falls within the range derived in anoxic soil incubations (11 to 33‰)
(Mariotti et al., 1982) and is consistent with results based on denitrifying bacteria carrying copper-containing NIR
(22‰) (Martin and Casciotti, 2016). Under both model scenarios, the best-fit ¹⁵η_{NOR} (-8 to 2‰) is relatively small
and more normal than the bulk N isotope effect for NO reduction to N₂O catalyzed by purified fungal NOR
(P450nor) (-14‰) (Yang et al., 2014). During P450nor-catalyzed NO reduction, two NO molecules are sequentially
625 bonded to the Fe active site of P450nor and the observed inverse isotope effect was proposed to arise from a
reversible bonding of the first NO molecule (Yang et al., 2014). To date, the N isotope effect for NO reduction
catalyzed by bacterial NORs has not yet been quantified. Unlike P450nor, which contains only a single heme Fe at
the active site, the active site of bacterial NORs has two Fe atoms (i.e., binuclear center). Therefore, three classes of
630 mechanisms have been proposed for the two-electron reduction of NO by bacterial NORs, including sequential
bonding of two NO molecules to either Fe catalytic center and simultaneous bonding of two NO molecules to both
Fe centers (Kuypers et al., 2018; Lehnert et al., 2018). Although the precise catalytic mechanism remains uncertain,
site-specific measurements of N isotopes in N₂O (i.e., N₂O isotopomers) produced from denitrifying bacteria
indicate similar magnitude for isotopic fractionations during the reduction of two NO molecules, in support of the
635 simultaneous binding theory (Sutka et al., 2006; Yamazaki et al., 2014). Thus, if the bulk N isotope effect for
bacterial NO reduction is higher than that for fungal NO reduction, the best-fit ¹⁵η_{NOR} may reflect a mixed
contribution of bacteria and fungi to NO consumption during the anoxic incubation. Alternatively, the model-
inferred ¹⁵η_{NOR} might reflect a balance between enzymatic and diffusion isotope effects, as has been previously
demonstrated for N₂O reduction in soil denitrification (Lewicka-Szczebak et al., 2014). Because diffusion would be
640 expected to have a small and normal kinetic isotope effect, if NO₂⁻ reduction was limited by NO diffusion out of soil
denitrifying sites, the estimated ¹⁵η_{NOR} would be shifted toward the isotope effect for NO diffusion. Diffusion might
be particularly important in this study due to the flow-through condition during the anoxic incubation and the low
solubility of NO, both of which favor gas diffusion while preventing re-entry of escaped NO to denitrifying cells.
Thus, the small ¹⁵η_{NOR} inferred from the best-fit models is likely a combination of diverse NO reduction pathways in
645 this agricultural soil, as well as limited expression of enzymatic isotope effects imposed by NO diffusion.
Regardless, the empirical finding of this study suggests that due to the small ¹⁵η_{NOR}, the bulk δ¹⁵N values of
denitrification-produced N₂O should not be significantly altered by accumulation and diffusion of NO during
denitrification.



650 4.3 NO source contribution and N isotope effects for NO production from NH₄⁺ oxidation under oxic and hypoxic conditions

The coupled decrease in NH₄⁺ concentrations and increase in NO₃⁻ concentrations (Fig. 3a and 3b) indicate active nitrification in both oxic and hypoxic incubations. Moreover, the two oxidation steps of nitrification were tightly coupled, resulting in no accumulation of NO₂⁻ in the soil. Because NO₃⁻ produced from nitrification has a zero Δ¹⁷O value, the active nitrification was also reflected in the progressive dilution of Δ¹⁷O-NO₃⁻ under both oxic and hypoxic conditions (Yu and Elliott, 2018). Based on the measured concentrations and isotopic composition of NH₄⁺ and NO₃⁻, the isotopologue-specific model previously developed by Yu and Elliott (2018) was used to estimate the rates and net N isotope effects of net mineralization ($R_{\text{OrgN/NH}_4}$ and $^{15}\eta_{\text{OrgN/NH}_4}$), gross NH₄⁺ oxidation to NO₃⁻ ($R_{\text{NH}_4/\text{NO}_3}$ and $^{15}\eta_{\text{NH}_4/\text{NO}_3}$), and gross NO₃⁻ consumption ($R_{\text{NO}_3\text{comp}}$ and $^{15}\eta_{\text{NO}_3\text{comp}}$) during the oxic and hypoxic incubations. As have been discussed above, this numerical model relies on the conservative nature of Δ¹⁷O-NO₃⁻ and its powerful applications in tracing co-occurring nitrification and NO₃⁻ consumption (consisting of NO₃⁻ immobilization and denitrification in this case) (Yu and Elliott, 2018). Detailed model derivation, formulation, and optimization have been documented in Yu and Elliott (2018) and are also briefly summarized in Text S5 in the Supplement. The modeling results based on the low δ¹⁵N-NH₄⁺ treatment in the oxic incubation were reported by Yu and Elliott (2018). Here, we used data from all three δ¹⁵N-NH₄⁺ treatments to more robustly constrain the N transformation rates and net N isotope effects for each incubation experiment (i.e., oxic and hypoxic).

The modeling results were summarized in Table 2. Excellent agreement was obtained between the observed and simulated concentrations and isotopic composition of NH₄⁺ and NO₃⁻ for both oxic and hypoxic incubations (Fig. 3). $R_{\text{NH}_4/\text{NO}_3}$ can be well described by zero order kinetics and was estimated to be 0.46 μg N·g⁻¹·h⁻¹ and 0.11 μg N·g⁻¹·h⁻¹ for the oxic and hypoxic incubations, respectively (Table 2). The lower $R_{\text{NH}_4/\text{NO}_3}$ in the hypoxic incubation indicates that nitrification was limited by low O₂ availability. Under both oxic and hypoxic conditions, oxidation of NH₄⁺ to NO₃⁻ was associated with a large $^{15}\eta_{\text{NH}_4/\text{NO}_3}$ (23 to 28‰; Table 2), consistent with the N isotope effects for NH₃ oxidation in pure cultures of AOB and AOA (e.g., 13 to 41‰) (Mariotti et al., 1981; Casciotti et al., 2003; Santoro et al., 2011). On the other hand, the estimated $R_{\text{OrgN/NH}_4}$ and $R_{\text{NO}_3\text{comp}}$ were low and not significantly different between the two incubation experiments (Table 2). Nevertheless, while $R_{\text{NO}_3\text{comp}}$ was only 16% of $R_{\text{NH}_4/\text{NO}_3}$ in the oxic incubation, $R_{\text{NO}_3\text{comp}}$ accounted for a much larger fraction (63%) of $R_{\text{NH}_4/\text{NO}_3}$ in the hypoxic incubation, mainly due to the reduced $R_{\text{NH}_4/\text{NO}_3}$ under the low O₂ condition. Due to the low magnitude of $R_{\text{OrgN/NH}_4}$ and $R_{\text{NO}_3\text{comp}}$, the estimated $^{15}\eta_{\text{OrgN/NH}_4}$ and $^{15}\eta_{\text{NO}_3\text{comp}}$ are associated with large errors and not significantly different from zero (Table 2).

By using three isotopically different NH₄⁺ fertilizers in parallel treatments, we are able to quantify the fractional contribution of NH₄⁺ oxidation to the measured net NO production (f_{NH_4}). Specifically, if NO was exclusively produced from soil NH₄⁺, we would expect to see a constant δ¹⁵N difference between NH₄⁺ and NO across the three δ¹⁵N-NH₄⁺ treatments. In fact, the observed δ¹⁵N differences were not constant and the slope of δ¹⁵N-NH₄⁺ versus δ¹⁵N-NO was significantly lower than unity under both oxic and hypoxic conditions (Fig. 4). This suggests that sources other than NH₄⁺ oxidation contributed to the observed net NO production. Although NO can be produced by numerous microbial and abiotic processes (Medinets et al., 2015), we argue that the other major NO



source is mostly likely related to NO_3^- consumption. This is based on the observation of high NO_3^- concentrations in both oxic and hypoxic incubations, as well as the estimated low $R_{\text{OrgN}/\text{NH}_4}$ (Table 2), which indicates a low availability of labile organic N – another potential substrate for NO production (Stange et al., 2013) – in this agricultural soil. Therefore, based on the assumption that NH_4^+ oxidation and NO_3^- consumption were the two primary NO sources during the oxic and hypoxic incubations, a two-source isotope mixing model was used to relate the measured $\delta^{15}\text{N}\text{-NO}$ values to the concurrently measured $\delta^{15}\text{N}\text{-NH}_4^+$ and $\delta^{15}\text{N}\text{-NO}_3^-$ values:

$$\delta^{15}\text{N}\text{-NO} = f_{\text{NH}_4} \times (\delta^{15}\text{N}\text{-NH}_4^+ - {}^{15}\eta_{\text{NH}_4/\text{NO}}) + (1 - f_{\text{NH}_4}) \times (\delta^{15}\text{N}\text{-NO}_3^- - {}^{15}\eta_{\text{NO}_3/\text{NO}}) \quad \text{Equation (5)}$$

where ${}^{15}\eta_{\text{NH}_4/\text{NO}}$ and ${}^{15}\eta_{\text{NO}_3/\text{NO}}$ are the net isotope effects for NO production from NH_4^+ oxidation and NO_3^- consumption, respectively. Rearranging Equation (5) yields Equation (6):

$$\delta^{15}\text{N}\text{-NO} = f_{\text{NH}_4} \times \delta^{15}\text{N}\text{-NH}_4^+ + (1 - f_{\text{NH}_4}) \times \delta^{15}\text{N}\text{-NO}_3^- - [f_{\text{NH}_4} \times {}^{15}\eta_{\text{NH}_4/\text{NO}} + (1 - f_{\text{NH}_4}) \times {}^{15}\eta_{\text{NO}_3/\text{NO}}] \quad \text{Equation (6)}$$

$${}^{15}\eta_{\text{comb}} = f_{\text{NH}_4} \times {}^{15}\eta_{\text{NH}_4/\text{NO}} + (1 - f_{\text{NH}_4}) \times {}^{15}\eta_{\text{NO}_3/\text{NO}} \quad \text{Equation (7)}$$

$$\delta^{15}\text{N}\text{-NO} = f_{\text{NH}_4} \times \delta^{15}\text{N}\text{-NH}_4^+ + (1 - f_{\text{NH}_4}) \times \delta^{15}\text{N}\text{-NO}_3^- - {}^{15}\eta_{\text{comb}} \quad \text{Equation (8)}$$

Equation (6) essentially dictates that the $\delta^{15}\text{N}\text{-NO}$ values can be modeled from the $\delta^{15}\text{N}\text{-NH}_4^+$ and $\delta^{15}\text{N}\text{-NO}_3^-$ values using a hypothetical isotope effect for NO production from the combined soil NH_4^+ and NO_3^- pool (${}^{15}\eta_{\text{comb}}$; the last term in Equation (6)) that is a mixing of ${}^{15}\eta_{\text{NH}_4/\text{NO}}$ and ${}^{15}\eta_{\text{NO}_3/\text{NO}}$ controlled by f_{NH_4} (Equation 7). Thus, assuming f_{NH_4} and ${}^{15}\eta_{\text{comb}}$ were constant in each incubation experiment, f_{NH_4} and ${}^{15}\eta_{\text{comb}}$ can be solved using the measured $\delta^{15}\text{N}\text{-NO}$, $\delta^{15}\text{N}\text{-NH}_4^+$, and $\delta^{15}\text{N}\text{-NO}_3^-$ values from all three $\delta^{15}\text{N}\text{-NH}_4^+$ treatments (Equation 8). f_{NH_4} was estimated to be 0.72 under the oxic incubation (Table 2), indicating that 72% of the measured net NO production was sourced from NH_4^+ oxidation, with the remainder being ascribed to NO_3^- consumption. Under the hypoxic condition, the share of NH_4^+ oxidation decreased to 58% (Table 2). ${}^{15}\eta_{\text{comb}}$ was estimated to be 56‰ under the oxic condition and 51‰ under the hypoxic condition (Table 2). Combining the $\delta^{15}\text{N}$ -based NO source partitioning with the estimated $R_{\text{NH}_4/\text{NO}_3}$ and $R_{\text{NO}_3/\text{comp}}$, we further estimated NO yield in NH_4^+ oxidation and NO_3^- consumption, respectively, and where the results are illustrated according to the classic “hole-in-the-pipe” (HIP) concept (Fig 9) (Davidson and Verchot, 2000). NO yield was 1.3% in NH_4^+ oxidation and 3.2% in NO_3^- consumption in the oxic incubation (Fig. 9; Table 2). Under the hypoxic condition, NO yield was increased to 5.2% in NH_4^+ oxidation and 6.1% in NO_3^- consumption (Fig. 9; Table 2).

Most previous laboratory and field studies suggest that soil NO emissions are predominately driven by nitrification, whereas NO produced from denitrification is further reduced to N_2O before it escapes to the soil surface (Kester et al., 1997; Skiba et al., 1997). The minor role of denitrification is largely deduced from the supposition that denitrification is activated only under wet soil conditions (Davidson and Verchot, 2000). However, based on our $\delta^{15}\text{N}$ -based NO source partitioning, about 30% of the net NO production was contributed by NO_3^- consumption under oxic condition, highlighting the potential importance of denitrification in driving soil NO emissions under conditions not typically conducive to its occurrence. There is growing evidence that extensive anoxic microsites can develop in otherwise well-aerated soils due to micro-scale variability of O_2 demand and soil texture-dependent gas diffusion limitations (Keiluweit et al. 2018). Although we would not predict high rates of heterotrophic respiration in this agricultural soil with low organic carbon, it is possible that rapid O_2 consumption by nitrification may outpace O_2 supply through diffusion in soil microsites, fostering development of anoxic niches in



close association with nitrification hot spots (Kremen et al., 2005). Based on ^{15}N labeling and direct ^{15}NO measurements using a gas chromatograph-quadrupole mass spectrometer, Russow et al. (2009) demonstrated that nitrification contributed about 70% of net NO production in a well-aerated, NH_4^+ -fertilized silt loam, in strong agreement with our results based on natural abundance $\delta^{15}\text{N}$ measurements. An even lower contribution to NO production, e.g., 26 to 44%, has been reported for nitrification in organic, N-enrich forest soils incubated under oxic conditions (Stange et al., 2013). The persistence of denitrifying microsites in the studied soil is further corroborated by the nearly doubled net NO production from NO_3^- consumption in the hypoxic incubation (Fig. 9). Importantly, the actual NO yield in denitrification might be much higher than those estimated for gross NO_3^- consumption during the oxic and hypoxic incubations (i.e., 3.2% and 6.1%), as denitrification occurring in anoxic niches might only comprise a small fraction of the estimated $R_{\text{NO}_3\text{comp}}$.

Interestingly, while $R_{\text{NH}_4/\text{NO}_3}$ was significantly lower in the hypoxic incubation, the net NO production from NH_4^+ oxidation was similar between the two incubation experiments, indicating a higher NO yield in nitrification when O_2 availability became limited (Fig. 9). However, mechanisms underlying the differential NO yield in nitrification are difficult to elucidate owing to the high complexity of biochemical pathways of NO production by AOB and AOA. In AOB, the prevailing view of NH_3 oxidation is that it occurs via a two-step enzymatic process, involving hydroxylamine (NH_2OH) as an obligatory intermediate (Fig. 10). The first step is catalyzed by NH_3 monooxygenase (AMO), which uses copper and O_2 to hydroxylate NH_3 to NH_2OH . Next, a multiheme enzyme, NH_2OH oxidoreductase (HAO), catalyzes the four-electron oxidation of NH_2OH to NO_2^- via enzyme-bound nitroxyl ([HNO-Fe]) and nitrosyl ([NO-Fe]) intermediates (Lehnert et al., 2018) (Fig. 10). Under this ‘ NH_2OH obligate intermediate’ model, NO emission was proposed to result from dissociation of NO from the enzyme-bound nitrosyl complex under high NH_3 and/or low O_2 conditions (Fig. 10) (Hooper et al., 2005; Beeckman et al., 2018). However, there is recent strong evidence that HAO generally catalyzes the three-electron oxidation of NH_2OH to NO under both aerobic and anaerobic conditions; the HAO-produced NO is further oxidized to NO_2^- by an unknown enzyme (Caranto et al., 2017). In this way, NO would not be a byproduct of incomplete NH_2OH oxidation, but rather required as an obligatory intermediate for NO_2^- production (Fig. 10). It was further proposed that AOB-encoded copper-containing NIR may catalyze the final one-electron oxidation of NO to NO_2^- by operating in reverse (Lancaster et al., 2018). Under this ‘ $\text{NH}_2\text{OH}/\text{NO}$ obligate intermediate’ model, high intracellular NO concentrations arise when the rate of NO production outpaces the rate of its oxidation to NO_2^- , leading to NO leakage from cells. Consequently, under O_2 stress, decreases in the rate of NO oxidation to NO_2^- might be expected, and this may explain the observed increase in nitrification NO yield in the hypoxic incubation. Additionally, some AOB strains can produce NO in a process termed ‘nitrifier-denitrification’, in which NO is produced through NIR-catalyzed NO_2^- reduction and can be further reduced to N_2O by AOB-encoded NOR (Wrage-Mönning et al., 2018) (Fig. 10). Compared to AOB, the NH_3 oxidation pathway in AOA remains unclear (Beeckman et al., 2018). The current model is that NH_3 is first oxidized by an archaeal AMO to NH_2OH and subsequently converted to NO_2^- by an unknown HAO counterpart (Kozłowski et al., 2016). NO seems to be mandatory for archaeal NH_2OH oxidation and has been proposed to act as a co-substrate for the NO_2^- production (Kozłowski et al., 2016). Consequently, NO is usually produced and immediately consumed with tighter control in AOA than in AOB (Kozłowski et al., 2016).



760 To shed further light on the inner workings of net NO production from NH_4^+ , we turn to constraining
 $^{15}\eta_{\text{NH}_4/\text{NO}}$. Specifically, the inherent linkage between $^{15}\eta_{\text{comb}}$, $^{15}\eta_{\text{NH}_4/\text{NO}}$, and $^{15}\eta_{\text{NO}_3/\text{NO}}$ (Equation 7) allows one to
probe the relative magnitude of $^{15}\eta_{\text{NH}_4/\text{NO}}$ and $^{15}\eta_{\text{NO}_3/\text{NO}}$ using the determined $^{15}\eta_{\text{comb}}$ and f_{NH_4} . Given that NO_2^- was
absent in the soil and that NO reduction in denitrification was likely associated with a small isotope effect (i.e.,
 $^{15}\eta_{\text{NOR}}$; see above), $^{15}\eta_{\text{NO}_3/\text{NO}}$ in the oxic and hypoxic incubations should mainly reflect $^{15}\eta_{\text{NAR}}$. Thus, by assigning
765 the entire possible range of the best-fit $^{15}\eta_{\text{NAR}}$ derived in the anoxic incubation (5 to 45‰; Fig. 7a) to $^{15}\eta_{\text{NO}_3/\text{NO}}$,
 $^{15}\eta_{\text{NH}_4/\text{NO}}$ was estimated to range from 60 to 76‰ in the oxic incubation and from 55 to 84‰ in the hypoxic
incubation (Fig. 11). If we take one step further by assuming that both $^{15}\eta_{\text{NO}_3/\text{NO}}$ and $^{15}\eta_{\text{NH}_4/\text{NO}}$ were identical between
the oxic and hypoxic incubations, then $^{15}\eta_{\text{NO}_3/\text{NO}}$ and $^{15}\eta_{\text{NH}_4/\text{NO}}$ could be uniquely determined to be 30‰ and 66‰,
respectively (Fig. 11; Table 2). Thus, the relative magnitude of $^{15}\eta_{\text{NO}_3/\text{NO}}$ and $^{15}\eta_{\text{NH}_4/\text{NO}}$ provides insights into the
770 differential relationship between $\delta^{15}\text{N-NH}_4^+$ and $\delta^{15}\text{N-NO}$ across the three $\delta^{15}\text{N-NH}_4^+$ treatments in the oxic and
hypoxic incubations (Fig. 4). In the oxic incubation, if we assume that $^{15}\eta_{\text{NH}_4/\text{NO}} = 66\text{‰}$ and $^{15}\eta_{\text{NO}_3/\text{NO}} = 30\text{‰}$, the
 $\delta^{15}\text{N}$ of NO produced from NH_4^+ oxidation under the low $\delta^{15}\text{N-NH}_4^+$ treatment (about -60‰) would be much lower
than the $\delta^{15}\text{N}$ of NO from NO_3^- consumption (about -38‰). However, under the high $\delta^{15}\text{N-NH}_4^+$ treatment, the $\delta^{15}\text{N}$
of NH_4^+ -produced NO would increase to about -14‰ and be higher than $\delta^{15}\text{N}$ values of NO_3^- -produced NO (about -
775 26‰). Consequently, the production of NO from NO_3^- consumption would “dilute” the $\delta^{15}\text{N}$ of total net NO
production, pulling it to fall below the 1:1 line between the $\delta^{15}\text{N-NH}_4^+$ and $\delta^{15}\text{N-NO}$ values in Fig. 4. This “dilution
effect” was more pronounced in the hypoxic incubation due to the lower f_{NH_4} (i.e., higher contribution of NO_3^- -
produced NO) (Fig. 4).

Therefore, under either oxic or hypoxic condition, the net NO production from NH_4^+ oxidation proceeded
780 with a large $^{15}\eta_{\text{NH}_4/\text{NO}}$. As NH_3 oxidation to NH_2OH was likely the rate-limiting step for the entire nitrification
process, a fraction of the inferred large $^{15}\eta_{\text{NH}_4/\text{NO}}$ can be accounted for by the isotope effect for NH_3 oxidation to
 NH_2OH , which should be similar to the estimated $^{15}\eta_{\text{NH}_4/\text{NO}_3}$ (e.g., 23 to 28‰). The residual isotope effect, on the
order of 40‰, must therefore stem from additional bond forming/breaking during net NO production in NH_3
oxidation. This additional N isotope effect could be explained by NO_2^- reduction catalyzed by AOB-encoded NIR if
785 NO was dominantly produced through the nitrifier-denitrification pathway (Fig. 10). However, provided that the two
oxidation steps of nitrification were tightly coupled under both oxic and hypoxic conditions, it is unlikely that NO_2^-
would accumulate to high enough intracellular concentrations to trigger nitrifier-denitrification (Wrage-Mönning et
al., 2018). Similarly, we would not expect any substantial fractionations to result from accumulation of intracellular
 NH_2OH or enzyme-bound intermediate species (e.g., $[\text{HNO-Fe}]$ and $[\text{NO-Fe}]$). Thus, we are left with either a large
790 and normal isotope effect for NO dissociation from its enzyme-bound precursor if NO production was mainly routed
through the ‘ NH_2OH obligate intermediate’ pathway or an inverse isotope effect associated with NO oxidation if
NO itself was an obligatory intermediate required for NO_2^- production (Fig. 10). With respect to the first possibility,
if NO dissociation from the Fe active site of HAO is mainly controlled by an equilibrium reaction between NO and
enzyme-bound nitrosyl species, the forward and backward reactions may occur with distinctively different isotope
795 effects, giving rise to an equilibrium isotope effect that favors partitioning of ^{14}N to the dissociated NO. However,
expression of this equilibrium isotope effect would be largely suppressed by limited isotope exchange between the



two N pools due to the presumably transient presence of nitrosyl intermediate. Therefore, a partial expression of a large equilibrium isotope effect (e.g., > 40‰) would be required to explain the residual N isotopic fractionation during NO production in NH₃ oxidation. Alternatively, in regards to the second possibility, if we assume that the enzyme-catalyzed oxidation of NO to NO₂⁻ proceeds via an enzyme-bound transition state and that the transition state contains the newly formed N-O bond, an inverse isotope effect may result from more strongly bonded N atom in the transition state, for which there is precedent in the literature (i.e., NO₂⁻ oxidation to NO₃⁻; see above) (Casciotti et al., 2009). Moreover, the small NO yield observed in the oxic and hypoxic incubations would indicate a large consumption of NO (i.e., 95 to 99%). With this high level of NO consumption, an inverse isotope effect on the order of -13 to -9‰ would be sufficient to account for the residual isotope effect for net NO production from NH₄⁺. This inferred isotope effect is of similar magnitude to that reported for NXR-catalyzed NO₂⁻ oxidation (i.e., -13‰) (Casciotti et al., 2009). However, to unambiguously determine the mechanisms giving rise to the large ¹⁵η_{NH₄/NO}, further biochemical analyses will be needed to clarify the enzymatic pathways responsible for NO production by AOB and AOA under relevant soil conditions. Nonetheless, the results presented here provide evidence that production of NO with low δ¹⁵N values may be a characteristic feature of nitrification in NH₄⁺-fertilized agricultural soils under both oxic and hypoxic conditions.

5 Implications for NO emission from agricultural soils

In this study, the net production rates and δ¹⁵N values of NO were measured under a range of controlled laboratory conditions. The results provide insights into how stable N and O isotopes can be effectively used to understand the reaction mechanisms by which NO is produced and consumed in soils. While nitrification is the commonly cited source for NO emissions from agricultural soils, the measured net NO production rates in this study highlight the great potential of abiotic NO₂⁻ reduction and denitrification in driving NO production and release from agricultural soils and thus should not be overlooked when attributing field soil NO emissions. Indeed, because NO is a direct product or free intermediate in these processes, abiotic NO₂⁻ reduction and denitrification may inherently have a larger NO yield – that is, a bigger “hole” for NO leaking in the HIP model (Davidson and Verchot, 2000). We conclude that the isotope-based measurement and modeling framework established in this work is a powerful tool to bridge NO production with gross N transformation processes in agricultural soils, thereby providing a quantitative way to parameterize the HIP model for modeling soil NO emissions under dynamic environmental conditions (e.g., varying temperature and soil moisture content).

The differences in the net isotope effects for NO production from abiotic NO₂⁻ reduction, denitrification, and nitrification revealed in this study (Fig. 12a) suggest that δ¹⁵N-NO is a useful tracer for informing NO production pathways in agricultural soils. Specifically, the relatively small magnitude of ¹⁵η_{NO₂/NO(abiotic)} indicates that δ¹⁵N-NO is particularly useful in probing the relative importance of NO production from abiotic versus microbial reactions, lending support to our previous finding based on rewetting of a dry forest soil that high δ¹⁵N values of rewetting-triggered NO pulses was mainly contributed by chemical NO₂⁻ reduction (Yu and Elliott, 2017). Moreover, the large ¹⁵η_{NH₄/NO} revealed in the oxic and hypoxic incubations provides an empirical basis for discerning the relative role of NH₄⁺ oxidation and NO₃⁻ reduction in driving soil NO production and emissions.



835 Interestingly, comparing the measured net isotope effects for NO production from abiotic NO₂⁻ reduction, denitrification, and nitrification with those previously quantified for N₂O production in soil incubations and pure cultures (Denk et al., 2017 and references therein; Jones et al., 2015; Wei et al., 2019), a similar pattern is evident across these three common production pathways for NO and N₂O (Fig. 12a). This similarity reflects the intimate connection between NO and N₂O turnovers within each reaction pathway and provides strong evidence that simultaneous δ¹⁵N-NO and δ¹⁵N-N₂O measurements can potentially yield unprecedented insights into the sources and processes controlling NO and N₂O emissions from agricultural soils. However, on the other hand, the demonstrated reaction reversibility between NO₂⁻ and NO₃⁻ under anoxic conditions is a new complication that needs to be considered when using δ¹⁵N to examine soil NO and N₂O emissions. As NO₂⁻ is often accumulated in agricultural soils following fertilizer application (Venterea et al., 2020), expression of the equilibrium isotope effect between NO₂⁻ and NO₃⁻ in redox-dynamic surface soils may render δ¹⁵N-NO and δ¹⁵N-N₂O less useful in tracing NO and N₂O sources. Given that high soil NO₂⁻ concentrations can trigger emission pulses of NO and N₂O (Venterea et al., 2020), NO₂⁻ accumulation should be taken as a critical sign for careful evaluation of the reaction complexity underlying δ¹⁵N distributions among the denitrification products.

To further assess the potential utility of δ¹⁵N measurements in source partitioning NO emissions from agricultural soils, we applied the estimated N isotope effects to the in situ δ¹⁵N-NO_x measurements reported by Miller et al. (2018). Importantly, the soil used in this study was collected from the same farm where Miller et al. (2018) conducted their field measurements (e.g., the USDA-managed corn-soybean field in central Pennsylvania, USA). Hence, the derived isotope effects may be particularly relevant to their reported δ¹⁵N-NO_x values due to similar soil microbial community structures. Because NO₂⁻ accumulation was not reported by Miller et al. (2018), we consider nitrification and denitrification to be the primary sources for the observed NO (and, to a much less extent, NO₂) emissions. Therefore, the ¹⁵η_{NH₄/NO and ¹⁵η_{NO₃/NO values derived in the oxic and hypoxic incubations (i.e., 66‰ and 30‰, respectively) were used in combination with the δ¹⁵N values of soil NH₄⁺ and NO₃⁻ reported in Miller et al. (2018) to calculate the δ¹⁵N endmembers for NO produced from NH₄⁺ oxidation and NO₃⁻ reduction. As shown in Fig. 12b, comparing the in situ δ¹⁵N-NO_x measurements with the estimated isotopic endmembers provides a compelling picture of soil NO dynamics following manure application. Notably, the initial low δ¹⁵N-NO_x values reported by Miller et al. (2018) might indicate a mixed contribution of NH₄⁺ oxidation and NO₃⁻ reduction to soil NO_x emissions (Fig. 12b). Nevertheless, the increase in δ¹⁵N-NO_x values measured 4 to 11 d after manure application may reflect a shift in dominant NO production pathway to denitrification, in line with the increasing accumulation of NO₃⁻ supplied by nitrification in the soil (Miller et al., 2018). Although data-limited, this example provides promising initial evidence for the ability of multi-species δ¹⁵N measurements to provide mechanistic information on soil NO dynamics and its environmental controls. Further experimental constraints on soil δ¹⁵N-NO variations can build on the measurement and modeling framework developed in this study to advance our understanding of soil NO source contributions over a wide range of environmental conditions and soil types.}}

Data availability. The datasets generated for this study and documentation about the equations and parameters of the isotopologue-specific models are available in the Supplement.



870

Supplement. The supplement related to this article is available online at:

Author contributions. Z.Y. and E.M.E. designed the study; Z.Y. conducted the experiments and analyzed the data; Z.Y. and E.M.E. wrote the paper.

875

Competing interests. The authors declare no conflict of interest.

880

Acknowledgements. The authors thank Dr. Curtis Dell (USDA-ARS) for helping with the field soil sampling, and Katherine Redling, Vivian Feng, Madeline Ellgass, and Madeline Gray (University of Pittsburgh) for assistance with the isotopic analyses.

Financial statement. This work was supported by a National Science Foundation CAREER award (Grant No. 1253000) to E.M.E.

References

- 885 Almaraz M., Bai E., Wang C., Trousdell J., Conley S., Faloona I. and Houlton B. Z.: Agriculture is a major source of NO_x pollution in California, *Sci. Adv.*, 4, 3477, 2018.
- Babbin A. R., Peters B. D., Mordy C. W., Widner B., Casciotti K. L. and Ward B. B.: Multiple metabolisms constrain the anaerobic nitrite budget in the Eastern Tropical South Pacific, *Global Biogeochem. Cycles*, 31, 258-271, 2017.
- 890 Beeckman F., Motte H. and Beeckman T.: Nitrification in agricultural soils: impact, actors and mitigation, *Curr. Opin. Biotechnol.*, 50, 166-173, 2018.
- Bock E., Wilderer, P. A. and Freitag A.: Growth of Nitrobacter in the absence of dissolved oxygen, *Water Res.*, 22, 245-250, 1988.
- Brunner B., Contreras S., Lehmann M. F., Matantseva O., Rollog M., Kalvelage T., Klockgether G., Lavik G., Jetten M. S., Kartal B. and Kuypers M. M.: Nitrogen isotope effects induced by anammox bacteria, *Proc. Natl. Acad. Sci. U.S.A.*, 110, 18994-18999, 2013.
- 895 Buchwald C. and Casciotti K. L.: Oxygen isotopic fractionation and exchange during bacterial nitrite oxidation, *Limnol. Oceanogr.*, 55, 1064-1074, 2010.
- Buchwald C., Grabb K., Hansel C. M. and Wankel S. D.: Constraining the role of iron in environmental nitrogen transformations: dual stable isotope systematics of abiotic NO₂⁻ reduction by Fe (II) and its production of N₂O, *Geochim. Cosmochim. Acta*, 186, 1-12, 2016.
- 900 Buchwald C., Homola K., Spivack A. J., Estes E. R., Murray R. W. and Wankel S. D.: Isotopic constraints on nitrogen transformation rates in the deep sedimentary marine biosphere, *Global Biogeochem. Cycles*, 32, 1688-1702, 2018.



- 905 Buessecker S., Tylor K., Nye J., Holbert K. E., Muñoz J. D. U., Glass J. B., Hartnett H. E. and Cadillo-Quiroz H.: Effects of sterilization techniques on chemodenitrification and N₂O production in tropical peat soil microcosms, *Biogeosciences*, 16, 4601-4612, 2019.
- Calvert J. G., Lazrus A., Kok G. L., Heikes B. G., Walega J. G., Lind J. and Cantrell C. A.: Chemical mechanisms of acid generation in the troposphere, *Nature*, 317, 27-35, 1985.
- 910 Caranto J. D. and Lancaster K. M.: Nitric oxide is an obligate bacterial nitrification intermediate produced by hydroxylamine oxidoreductase, *Proc. Natl. Acad. Sci. U.S.A.* 114, 8217-8222.
- Casciotti K. L.: Inverse kinetic isotope fractionation during bacterial nitrite oxidation, *Geochim. Cosmochim. Acta*, 73, 2061-2076, 2009.
- Casciotti K. L., Böhlke J. K., McIlvin M. R., Mroczkowski S. J. and Hannon J. E.: Oxygen isotopes in nitrite: analysis, calibration, and equilibration, *Anal. Chem.*, 79, 2427-2436, 2007.
- 915 Casciotti K. L., Sigman D. M., Hastings M. G., Böhlke J. K. and Hilkert A.: Measurement of the oxygen isotopic composition of nitrate in seawater and freshwater using the denitrifier method, *Anal. Chem.*, 74, 4905-4912, 2002.
- Casciotti K. L., Sigman D. M. and Ward B. B.: Linking diversity and stable isotope fractionation in ammonia-oxidizing bacteria, *Geomicrobiol. J.*, 20, 335-353, 2003.
- 920 Crutzen P. J.: The role of NO and NO₂ in the chemistry of the troposphere and stratosphere, *Annu. Rev. Earth and Planet. Sci.*, 7, 443-472, 1979.
- Davidson E.A.: The contribution of manure and fertilizer nitrogen to atmospheric nitrous oxide since 1860, *Nat. Geosci.*, 2, 659-662, 2009.
- 925 Dähnke K. and Thamdrup B.: Isotope fractionation and isotope decoupling during anammox and denitrification in marine sediments, *Limnol. Oceanogr.*, 61, 610-624, 2016.
- Dale A. W., Sommer S., Ryabenko E., Noffke A., Bohlen L., Wallmann K., Stolpovsky K., Greinert J. and Pfannkuche O.: Benthic nitrogen fluxes and fractionation of nitrate in the Mauritanian oxygen minimum zone (Eastern Tropical North Atlantic), *Geochim. Cosmochim. Acta*, 134, 234-256, 2014.
- 930 Davidson E. A. and Verchot L. V.: Testing the hole-in-the-pipe model of nitric and nitrous oxide emissions from soils using the TRAGNET database, *Global Biogeochem. Cycles*, 14, 1035-1043, 2000.
- Denk T. R., Mohn J., Decock C., Lewicka-Szczebak D., Harris E., Butterbach-Bahl K., Kiese R., and Wolf B.: The nitrogen cycle: A review of isotope effects and isotope modeling approaches, *Soil Biol. Biochem.*, 105, 121-137, 2017.
- 935 Felix D. J., Elliott E. M., Gish T. J., McConnell L. L. and Shaw S. L.: Characterizing the isotopic composition of atmospheric ammonia emission sources using passive samplers and a combined oxidation-bacterial denitrifier approach, *Rapid Commun. Mass Spectrom.*, 27, 2239-2246, 2013.
- Firestone M. K. and Davidson E. A.: Microbiological basis of NO and N₂O production and consumption in soil. In *Exchange of trace gases between terrestrial ecosystems and the atmosphere*; Andreae, M. O.; Schimel, D. S.; Robertson, G. P. Eds.; John Wiley & Sons Ltd: Berlin, pp 7-21, 1989.
- 940



- Freitag A., Rudert M. and Bock E.: Growth of Nitrobacter by dissimilatory nitrate reduction, *FEMS Microbiol. Lett.*, 48, 105-109, 1987.
- Friedman S. H., Masefski W. and Hollocher T. C.: Catalysis of intermolecular oxygen atom transfer by nitrite dehydrogenase of *Nitrobacter agilis*, *J. Biol. Chem.*, 261, 10538-10543, 1986.
- 945 Fry B.: *Stable Isotope Ecology* (Vol. 521). New York: Springer, 2006.
- Galloway J. N., Aber J. D., Erisman J. W., Seitzinger S. P., Howarth R. W., Cowling E. B. and Cosby B. J.: The nitrogen cascade, *Bioscience*, 53, 341-356, 2003.
- Gaye B., Nagel B., Dähnke K., Rixen T. and Emeis K.C.: Evidence of parallel denitrification and nitrite oxidation in the ODZ of the Arabian Sea from paired stable isotopes of nitrate and nitrite, *Global Biogeochem. Cycles*, 27, 1059-1071, 2013.
- 950 Granger J. and Sigman D. M.: Removal of nitrite with sulfamic acid for nitrate N and O isotope analysis with the denitrifier method, *Rapid Commun. Mass Spectrom.*, 23, 3753-3762, 2009.
- Granger J., Sigman D. M., Lehmann M. F. and Tortell P. D.: Nitrogen and oxygen isotope fractionation during dissimilatory nitrate reduction by denitrifying bacteria, *Limnol. Oceanogr.*, 53, 2533-2545, 2008.
- 955 Granger J. and Wankel S. D.: Isotopic overprinting of nitrification on denitrification as a ubiquitous and unifying feature of environmental nitrogen cycling, *Proc. Natl. Acad. Sci. U.S.A.*, 113, E6391-E6400, 2016.
- Heil J., Vereecken H. and Brüggemann N.: A review of chemical reactions of nitrification intermediates and their role in nitrogen cycling and nitrogen trace gas formation in soil, *Eur. J. Soil Sci.*, 67, 23-39, 2016.
- Højberg O., Binnerup S. J. and Sørensen J.: Potential rates of ammonium oxidation, nitrite oxidation, nitrate reduction and denitrification in the young barley rhizosphere, *Soil Biol. Biochem.*, 28, 47-54, 1996.
- 960 Homyak P. M., Vasquez K. T., Sickman J. O., Parker D. R. and Schimel J. P.: Improving nitrite analysis in soils: Drawbacks of the conventional 2 M KCl extraction, *Soil Sci. Soc. Am. J.*, 79, 1237-1242, 2015.
- Hooper A. B., Arciero D., Bergmann D. and Hendrich M. P.: The Oxidation of Ammonia as an Energy Source in Bacteria. In *Respiration in archaea and bacteria* (pp. 121-147). Springer, Dordrecht, 2004.
- 965 Hudman R. C., Moore N. E., Mebus A. K., Martin R. V., Russell A. R., Valin L. C. and Cohen R. C.: Steps towards a mechanistic model of global soil nitric oxide emissions: implementation and space based-constraints, *Atmos. Chem. Phys.*, 12, 7779-7795, 2012.
- Hudman R. C., Russell A. R., Valin L. C. and Cohen R. C.: Interannual variability in soil nitric oxide emissions over the United States as viewed from space, *Atmos. Chem. Phys.*, 10, 9943-9952, 2010.
- 970 Jones L. C., Peters B., Lezama Pacheco J. S., Casciotti K. L. and Fendorf S.: Stable isotopes and iron oxide mineral products as markers of chemodenitrification, *Environ. Sci. Technol.*, 49, 3444-3452, 2015.
- Kaiser J., Hastings M. G., Houlton B. Z., Röckmann T. and Sigman D. M.: Triple oxygen isotope analysis of nitrate using the denitrifier method and thermal decomposition of N₂O, *Anal. Chem.*, 79, 599-607, 2007.
- Kaneko M. and Poulson S. R.: The rate of oxygen isotope exchange between nitrate and water, *Geochim. Cosmochim. Acta*, 118, 148-156, 2013.
- 975 Kang H., Stanley E. H. and Park S. S.: A sensitive method for the measurement of ammonium in soil extract and water, *Commun. Soil Sci. Plant Anal.*, 34, 2193-2201, 2003.



- Ke X., Angel R., Lu Y. and Conrad R.: Niche differentiation of ammonia oxidizers and nitrite oxidizers in rice paddy soil, *Environ. Microbiol.*, 15, 2275-2292, 2013.
- 980 Keiluweit M., Gee K., Denney A. and Fendorf S.: Anoxic microsites in upland soils dominantly controlled by clay content, *Soil Biol. Biochem.*, 118, 42-50, 2018.
- Kemeny P. C., Weigand M. A., Zhang R., Carter B. R., Karsh K. L., Fawcett S. E. and Sigman D. M.: Enzyme-level interconversion of nitrate and nitrite in the fall mixed layer of the Antarctic Ocean, *Global Biogeochem. Cycles*, 30, 1069-1085, 2016.
- 985 Kester R. A., Meijer M. E., Libochant J. A., Boer W. D. and Laanbroek H. J.: Contribution of nitrification and denitrification to the NO and N₂O emissions of an acid forest soil, a river sediment and a fertilized grassland soil, *Soil Biol. Biochem.*, 29, 1655-1664, 1997.
- Koch H., Lücker S., Albertsen M., Kitzinger K., Herbold C., Spieck E., Nielsen P. H., Wagner M. and Daims H.: Expanded metabolic versatility of ubiquitous nitrite-oxidizing bacteria from the genus *Nitrospira*, *Proc. Natl. Acad. Sci. U.S.A.*, 112, 11371-11376, 2015.
- 990 Kool D. M., Wrage N., Oenema O., Van Kessel C. and Van Groenigen J. W.: Oxygen exchange with water alters the oxygen isotopic signature of nitrate in soil ecosystems, *Soil Biol. Biochem.*, 43, 1180-1185, 2011.
- Kozłowski J. A., Stieglmeier M., Schleper C., Klotz M. G. and Stein L. Y.: Pathways and key intermediates required for obligate aerobic ammonia-dependent chemolithotrophy in bacteria and Thaumarchaeota, *ISME J.*, 10, 1836-1845, 2016.
- 995 Kremen A., Bear J., Shavit U. and Shaviv A.: Model demonstrating the potential for coupled nitrification denitrification in soil aggregates, *Environ. Sci. Technol.*, 39, 4180-4188, 2005.
- Kuypers M. M., Marchant H. K. and Kartal B.: The microbial nitrogen-cycling network, *Nat. Rev. Microbiol.*, 16, 263, 2018.
- 1000 Lancaster K. M., Caranto J. D., Majer S. H. and Smith M. A.: Alternative bioenergy: updates to and challenges in nitrification metalloenzymology, *Joule*, 2, 421-441, 2018.
- Le Roux X., Bouskill N. J., Niboyet A., Barthes L., Dijkstra P., Field C. B., Hungate B. A., Lerondelle C., Pommier T., Tang J. and Terada A.: Predicting the responses of soil nitrite-oxidizers to multi-factorial global change: a trait-based approach, *Front. Microbiol.*, 7, 628, 2016.
- 1005 Lehnert N., Dong H. T., Harland J. B., Hunt A. P. and White C. J.: Reversing nitrogen fixation, *Nat. Rev. Chem.*, 2, 278-289, 2018.
- Lewicka-Szczebak D., Well R., Köster J. R., Fuß R., Senbayram M., Dittert K. and Flessa H.: Experimental determinations of isotopic fractionation factors associated with N₂O production and reduction during denitrification in soils, *Geochim. Cosmochim. Acta*, 134, 55-73, 2014.
- 1010 Li D. and Wang X.: Nitrogen isotopic signature of soil-released nitric oxide (NO) after fertilizer application, *Atmos. Environ.*, 42, 4747-4754, 2008.
- Lim N. Y., Frostegård Å. and Bakken L. R.: Nitrite kinetics during anoxia: The role of abiotic reactions versus microbial reduction, *Soil Biol. Biochem.*, 119, 203-209, 2018.



- 1015 Liu S., Lin F., Wu S., Ji C., Sun Y., Jin Y., Li S., Li Z. and Zou J.: A meta-analysis of fertilizer-induced soil NO and combined NO+N₂O emissions, *Global Change Biol.*, 23, 2520-2532, 2017.
- Loick N., Dixon E. R., Abalos D., Vallejo A., Matthews G. P., McGeough K. L., Well R., Watson C. J., Laughlin R. J. and Cardenas L. M.: Denitrification as a source of nitric oxide emissions from incubated soil cores from a UK grassland soil, *Soil Biol. Biochem.*, 95, 1-7, 2016.
- 1020 Maaz T. M., Waldo S., Bruulsema T. and Mikkelsen R.: Inconsistencies undermine the conclusion that agriculture is a dominant source of NO_x in California, *Sci. Adv.*, 4, 4706, 2018.
- Maggi F. and Riley W. J.: Mathematical treatment of isotopologue and isotopomer speciation and fractionation in biochemical kinetics, *Geochim. Cosmochim. Acta*, 74, 1823-1835, 2010.
- Mariotti A., Germon J. C., Hubert P., Kaiser P., Letolle R., Tardieux A., Tardieux P.: Experimental determination of nitrogen kinetic isotope fractionation: some principles; illustration for the denitrification and nitrification processes, *Plant Soil*, 62, 413-430, 1981.
- 1025 Mariotti A., Leclerc A. and Germon J. C.: Nitrogen isotope fractionation associated with the NO₂⁻→ N₂O step of denitrification in soils, *Can. J. Soil Sci.*, 62, 227-241, 1982.
- Martin T. S. and Casciotti K. L.: Nitrogen and oxygen isotopic fractionation during microbial nitrite reduction, *Limnol. Oceanogr.*, 61, 1134-1143, 2016.
- 1030 Martin T. S. and Casciotti K. L.: Paired N and O isotopic analysis of nitrate and nitrite in the Arabian Sea oxygen deficient zone, *Deep Sea Res. Part I*, 121, 121-131, 2017.
- McKenney D. J., Lazar C. and Findlay W. J.: Kinetics of the nitrite to nitric oxide reaction in peat, *Soil Sci. Soc. Am. J.*, 54, 106-112, 1990.
- McKenney D. J., Shuttleworth K. F., Vriesacker J. R. and Findlay W. I.: Production and loss of nitric oxide from denitrification in anaerobic Brookston clay, *Appl. Environ. Microbiol.*, 43, 534-541, 1982.
- 1035 Medinets S., Skiba U., Rennenberg H. and Butterbach-Bahl K.: A review of soil NO transformation: Associated processes and possible physiological significance on organisms, *Soil Biol. Biochem.*, 80, 92-117, 2015.
- Michalski G., Meixner T., Fenn M., Hernandez L., Sirulnik A., Allen E., Thiemens M.: Tracing atmospheric nitrate deposition in a complex semiarid ecosystem using Δ¹⁷O, *Environ. Sci. Technol.*, 38, 2175-2181, 2004.
- 1040 Miller D. J., Chai J., Guo F., Dell C. J., Karsten H. and Hastings M. G.: Isotopic Composition of In Situ Soil NO_x Emissions in Manure-Fertilized Cropland, *Geophys. Res. Lett.*, 45, 12-058, 2018.
- Peters B. D., Babbin A. R., Lettmann K. A., Mordy C. W., Ulloa O., Ward B. B. and Casciotti K. L.: Vertical modeling of the nitrogen cycle in the eastern tropical South Pacific oxygen deficient zone using high-resolution concentration and isotope measurements, *Global Biogeochem. Cycles*, 30, 1661-1681, 2016.
- 1045 Russow R., Stange C. F. and Neue H. U.: Role of nitrite and nitric oxide in the processes of nitrification and denitrification in soil: Results from ¹⁵N tracer experiments, *Soil Biol. Biochem.*, 41, 785-795, 2009.
- Santoro A. E. and Casciotti K. L.: Enrichment and characterization of ammonia-oxidizing archaea from the open ocean: phylogeny, physiology and stable isotope fractionation, *ISME J.* 5, 1796, 2011.
- Shoun H., Fushinobu S., Jiang L., Kim S. W. and Wakagi T.: Fungal denitrification and nitric oxide reductase cytochrome P450nor, *Philos. Trans. R. Soc. Ser. B*, 367, 1186-1194, 2012.
- 1050



- Sigman D. M., Casciotti K. L., Andreani M., Barford C., Galanter M. B. J. K. and Böhlke J. K.: A bacterial method for the nitrogen isotopic analysis of nitrate in seawater and freshwater, *Anal. Chem.*, 73, 4145-4153, 2001.
- Skiba U., Fowler D. and Smith K. A.: Nitric oxide emissions from agricultural soils in temperate and tropical climates: sources, controls and mitigation options, *Nutr. Cycling Agroecosyst.*, 48, 139-153, 1997.
- 1055 Stange C. F., Spott O., Arriaga H., Menéndez S., Estavillo J. M. and Merino P.: Use of the inverse abundance approach to identify the sources of NO and N₂O release from Spanish forest soils under oxic and hypoxic conditions, *Soil Biol. Biochem.*, 57, 451-458, 2013.
- Stein L. Y.: Insights into the physiology of ammonia-oxidizing microorganisms, *Curr. Opin. Chem. Biol.*, 49, 9-15, 2019.
- 1060 Sun X., Ji Q., Jayakumar A. and Ward B. B.: Dependence of nitrite oxidation on nitrite and oxygen in low-oxygen seawater, *Geophys. Res. Lett.*, 44, 7883-7891, 2017.
- Sutka R. L., Ostrom N. E., Ostrom P. H., Breznak J. A., Gandhi H., Pitt A. J. and Li F.: Distinguishing nitrous oxide production from nitrification and denitrification on the basis of isotopomer abundances, *Appl. Environ. Microbiol.*, 72, 638-644, 2006.
- 1065 Taylor A. E., Myrold D. D. and Bottomley P. J.: Temperature affects the kinetics of nitrite oxidation and nitrification coupling in four agricultural soils, *Soil Biol. Biochem.*, 136, 107523, 2019.
- Toyoda S., Yoshida N. and Koba K.: Isotopocule analysis of biologically produced nitrous oxide in various environments, *Mass Spectrom. Rev.*, 36, 135-160, 2017.
- Treibergs L. A. and Granger J.: Enzyme level N and O isotope effects of assimilatory and dissimilatory nitrate reduction, *Limnol. Oceanogr.*, 62, 272-288, 2017.
- 1070 Van Cleemput O. and Samater A. H.: Nitrite in soils: accumulation and role in the formation of gaseous N compounds, *Fert. Res.*, 45, 81-89, 1995.
- Veldkamp E. and Keller M.: Fertilizer-induced nitric oxide emissions from agricultural soils, *Nutr. Cycling Agroecosyst.*, 48, 69-77, 1997.
- 1075 Venterea R. T., Coulter J. A. and Clough T. J.: Nitrite accumulation and nitrogen gas production increase with decreasing temperature in urea-amended soils: Experiments and modeling, *Soil Biol. Biochem.*, 142, 107727, 2020.
- Venterea R. T., Rolston D. E. E. and Cardon Z. G.: Effects of soil moisture, physical, and chemical characteristics on abiotic nitric oxide production, *Nutr. Cycling Agroecosyst.*, 72, 27-40, 2005.
- 1080 Vinken G. C. M., Boersma K. F., Maasackers J. D., Adon M. and Martin R. V.: Worldwide biogenic soil NO_x emissions inferred from OMI NO₂ observations, *Atmos. Chem. Phys.*, 14, 10363-10381, 2014.
- Wei J., Ibraim E., Brüggemann N., Vereecken H. and Mohn J.: First real-time isotopic characterisation of N₂O from chemodenitrification, *Geochim. Cosmochim. Acta*, 267, 17-32, 2019.
- Wrage-Mönnig N., Horn M. A., Well R., Müller C., Velthof G. and Oenema O.: The role of nitrifier denitrification in the production of nitrous oxide revisited, *Soil Biol. Biochem.* 123, A3-A16, 2018.
- 1085



- Wunderlich A., Meckenstock R. U. and Einsiedl F.: A mixture of nitrite-oxidizing and denitrifying microorganisms affects the $\delta^{18}\text{O}$ of dissolved nitrate during anaerobic microbial denitrification depending on the $\delta^{18}\text{O}$ of ambient water, *Geochim. Cosmochim. Acta*, 119, 31-45, 2013.
- 1090 Yamazaki T., Hozuki T., Arai K., Toyoda S., Koba K., Fujiwara T. and Yoshida N.: Isotopomeric characterization of nitrous oxide produced by reaction of enzymes extracted from nitrifying and denitrifying bacteria, *Biogeosciences*, 11, 2679, 2014.
- Yang H., Gandhi H., Ostrom N. E. and Hegg E. L.: Isotopic fractionation by a fungal P450 nitric oxide reductase during the production of N_2O , *Environ. Sci. Technol.*, 48, 10707-10715, 2014.
- 1095 Ye R. W., Averill B. A. and Tiedje J. M.: Denitrification: production and consumption of nitric oxide, *Appl. Environ. Microbiol.*, 60, 1053, 1994.
- Yu Z. and Elliott E. M.: Novel method for nitrogen isotopic analysis of soil-emitted nitric oxide, *Environ. Sci. Technol.*, 51, 6268-6278, 2017.
- Yu Z. and Elliott E. M.: Probing soil nitrification and nitrate consumption using $\Delta^{17}\text{O}$ of soil nitrate, *Soil Biol. Biochem.*, 127, 187-199, 2018.
- 1100 Zhang L., Altabet M. A., Wu T. and Hadas O.: Sensitive measurement of NH_4^+ $^{15}\text{N}/^{14}\text{N}$ ($\delta^{15}\text{NH}_4^+$) at natural abundance levels in fresh and saltwaters, *Anal. Chem.*, 79, 5297-5303, 2007.
- Zhang S., Fang Y. and Xi D.: Adaptation of micro-diffusion method for the analysis of ^{15}N natural abundance of ammonium in samples with small volume, *Rapid Commun. Mass Spectrom.*, 29, 1297-1306, 2015.
- 1105 Zumft W. G.: Cell biology and molecular basis of denitrification, *Microbiol. Mol. Biol. Rev.*, 61, 533-616, 1997.



Tables

Table 1. Mean and 95% confidence interval of modeled denitrification rates and NO_2^- re-oxidation rate constant under the ‘no exchange’ and ‘complete exchange’ scenarios.

Parameter	Description	No exchange		Complete exchange	
		Mean	95% CI	Mean	95% CI
R_{NAR}	Zero order rate for NO_3^- reduction ($\mu\text{g N}\cdot\text{g}^{-1}\cdot\text{h}^{-1}$)	0.158	0.157 to 0.160	0.158	0.157 to 0.160
R_{NIR}	Zero order rate for NO_2^- reduction ($\mu\text{g N}\cdot\text{g}^{-1}\cdot\text{h}^{-1}$)	0.112	0.111 to 0.113	0.112	0.111 to 0.113
R_{NOR}	Zero order rate for NO reduction ($\mu\text{g N}\cdot\text{g}^{-1}\cdot\text{h}^{-1}$)	0.039	0.038 to 0.040	0.039	0.038 to 0.040
$k_{\text{NXR}(b)}$	First order rate constant of NO_2^- re-oxidation (h^{-1})	0.64	0.61 to 0.66	0.25	0.24 to 0.26



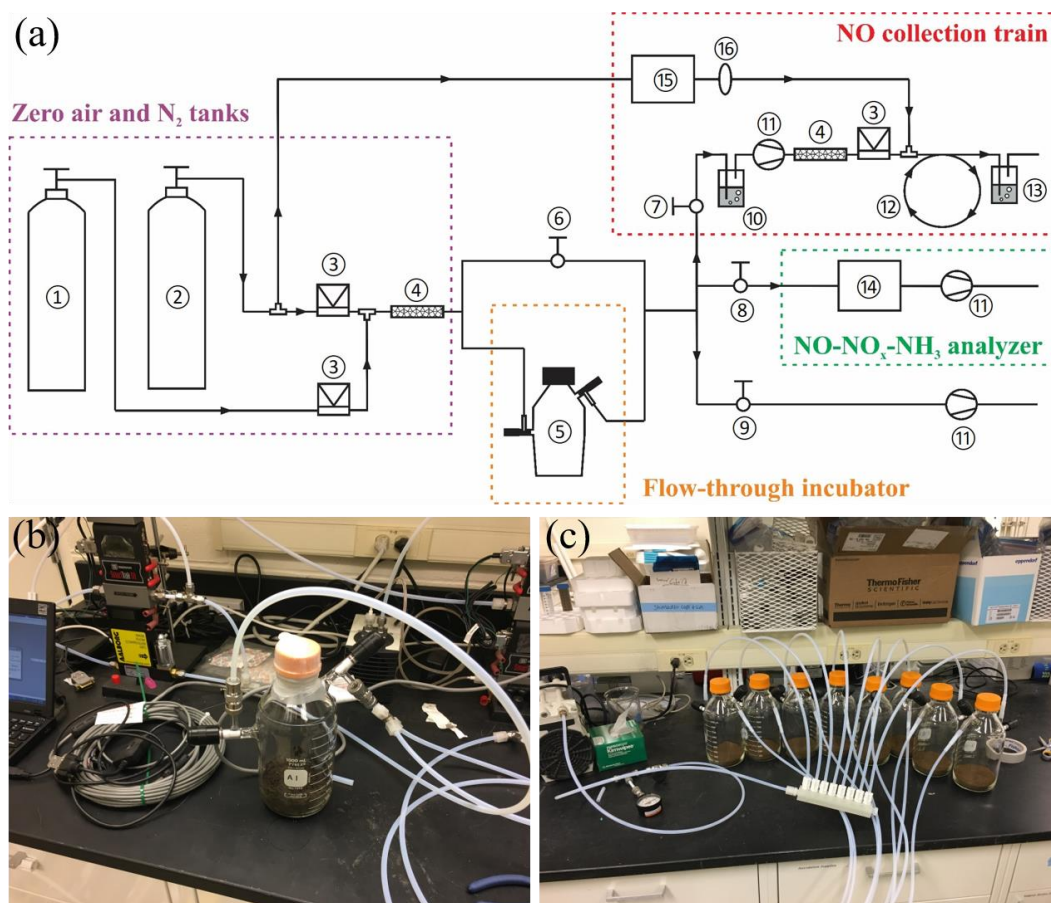
1110 Table 2. Mean and 95% confidence interval of modeled gross N transformation rates, NO yield, and net N isotope
 1111 effects in the oxic and hypoxic incubations.

Parameter	Description	Oxic		Hypoxic	
		Mean	95% CI	Mean	95% CI
$R_{\text{OrgN}/\text{NH}_4}$	Zero order rate for net mineralization ($\mu\text{g N}\cdot\text{g}^{-1}\cdot\text{h}^{-1}$)	0.014	0.013 to 0.016	0.012	-0.011 to 0.038
$R_{\text{NH}_4/\text{NO}_3}$	Zero order rate for gross nitrification ($\mu\text{g N}\cdot\text{g}^{-1}\cdot\text{h}^{-1}$)	0.458	0.455 to 0.460	0.111	0.110 to 0.113
$R_{\text{NO}_3\text{comp}}$	Zero order rate for gross NO_3^- consumption ($\mu\text{g N}\cdot\text{g}^{-1}\cdot\text{h}^{-1}$)	0.071	0.070 to 0.072	0.070	0.049 to 0.091
$^{15}\eta_{\text{OrgN}/\text{NH}_4}$	Net N isotope effect for net mineralization	2‰	-27 to 31‰	0‰	-18 to 17‰
$^{15}\eta_{\text{NH}_4/\text{NO}_3}$	Net N isotope effect for gross nitrification	28‰	27 to 30‰	23‰	12 to 33‰
$^{15}\eta_{\text{NO}_3\text{comp}}$	Net N isotope effect for gross NO_3^- consumption	5‰	-16 to 20‰	7‰	-9 to 23‰
f_{NH_4}	Fraction of net NO production from nitrification	0.72	0.65 to 0.78	0.58	0.55 to 0.61
$Y_{\text{NH}_4/\text{NO}}$	NO yield in nitrification	1.3%	1.2 to 1.4%	5.2%	4.8 to 5.5%
$Y_{\text{NO}_3/\text{NO}}$	NO yield in NO_3^- consumption	3.2%	2.5 to 4.0%	6.1%	4.3 to 9.3%
$^{15}\eta_{\text{comb}}$	Combined net isotope effect for NO production from NH_4^+ and NO_3^-	56‰	54 to 58‰	51‰	50 to 52‰
			Mean		95% CI
$^{15}\eta_{\text{NH}_4/\text{NO}}$	Net isotope effect for NO production from NH_4^+ oxidation		66‰		59 to 85‰
$^{15}\eta_{\text{NO}_3/\text{NO}}$	Net isotope effect for NO production from NO_3^- consumption		30‰		1 to 42‰

1112

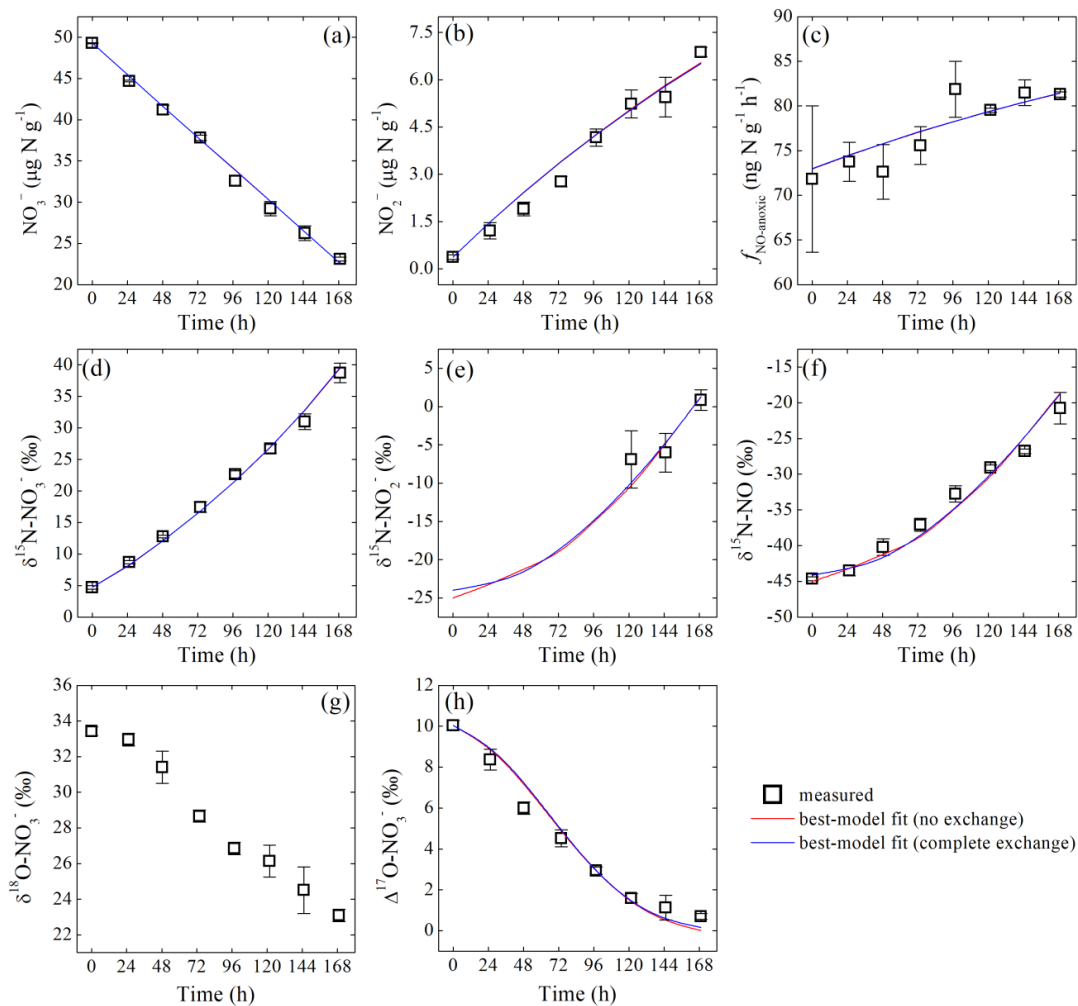


1113 **Figures**



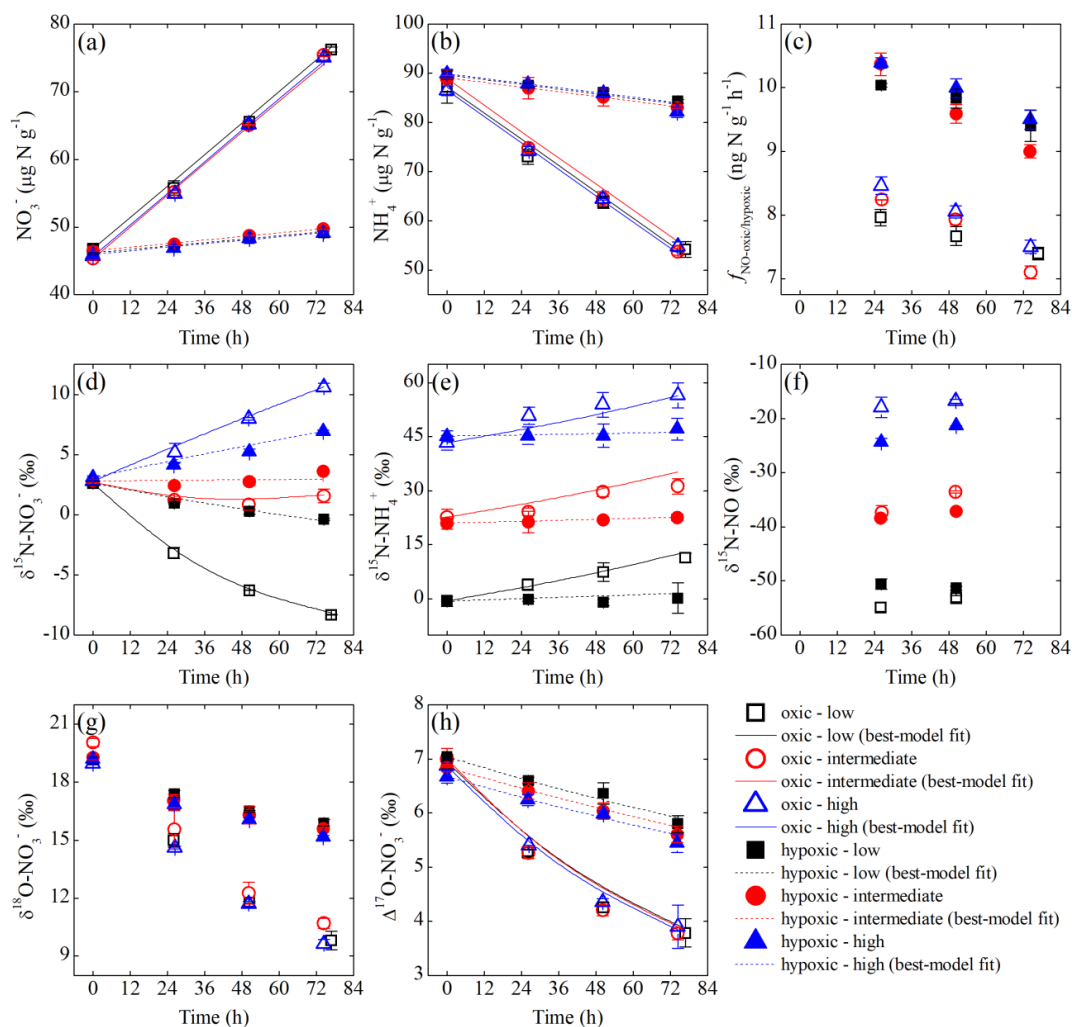
1114

1115 Figure 1. (a) Schematic of the DFC system (not to scale) consisting of the following: (1) zero air tank, (2) N₂ tank,
1116 (3) mass flow controller, (4) Nafion moisture exchanger, (5) flow-through incubator, (6) to (9) needle valves for
1117 controlling vacuum and flushing of the DFC system, (10) HONO scrubber, (11) diaphragm pump, (12) Teflon
1118 reaction tube, (13) gas washing bottle containing TEA solution, (14) NO-NO_x-NH₃ analyzer, (15) O₃ generator, (16)
1119 in-line PTFE particulate filter assembly. (b) Photo of the flow-through incubator. (c) Photo of the Teflon purging
1120 manifold for connection of the incubators in parallel.



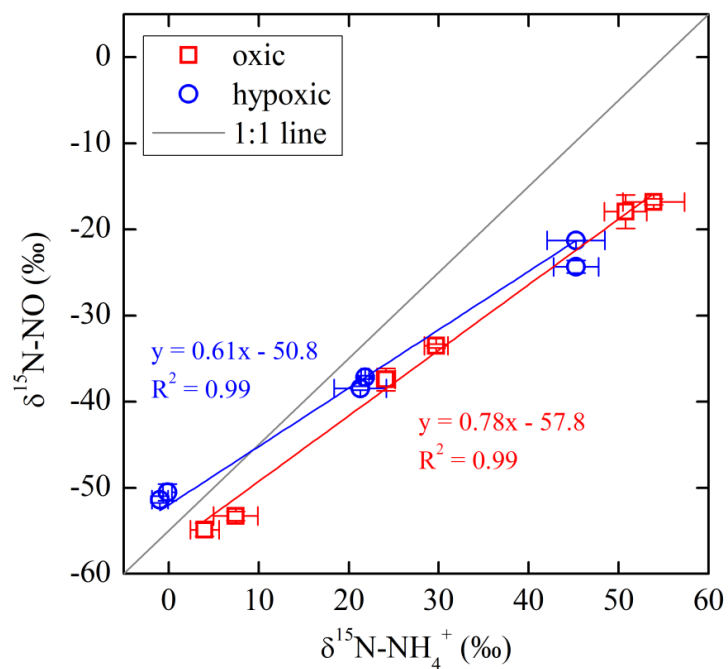
1121

1122 Figure 2. Measured and modeled concentrations of NO_3^- (a) and NO_2^- (b), net NO production rate (c),
1123 $\delta^{15}\text{N}$ values of NO_3^- (d), NO_2^- (e), and NO (f), and $\delta^{18}\text{O}$ (g) and $\Delta^{17}\text{O}$ (h) of NO_3^- during the anoxic
1124 incubation.



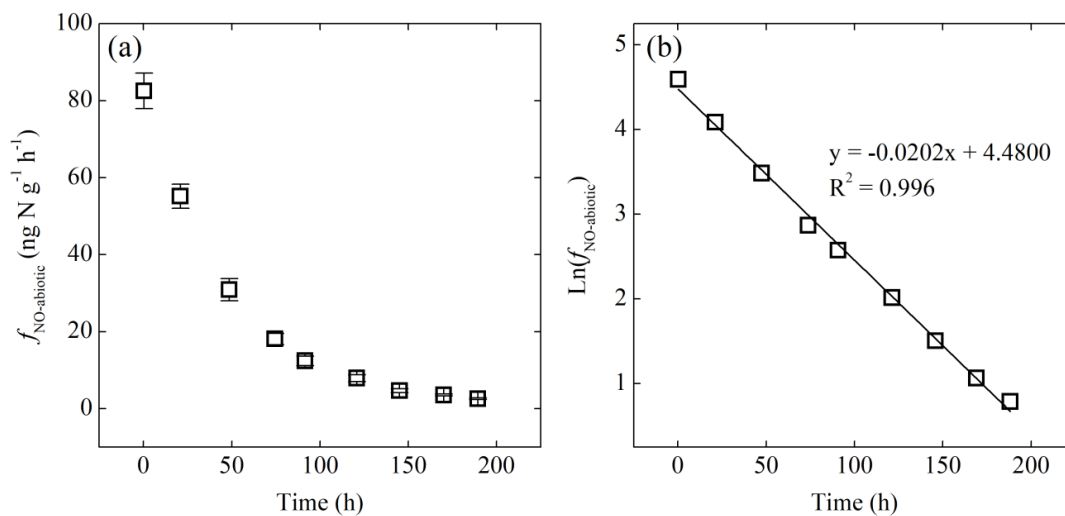
1125

1126 Figure 3. Measured and modeled concentrations of NO_3^- (a) and NH_4^+ (b), net NO production rate (c),
 1127 $\delta^{15}\text{N}$ values of NO_3^- (d) and NH_4^+ (e), and NO (f), and $\delta^{18}\text{O}$ (g) and $\Delta^{17}\text{O}$ (h) of NO_3^- under the three $\delta^{15}\text{N-}$
 1128 NH_4^+ treatments (differed by color) of the oxic (open symbols) and hypoxic (solid symbols) incubations.



1129

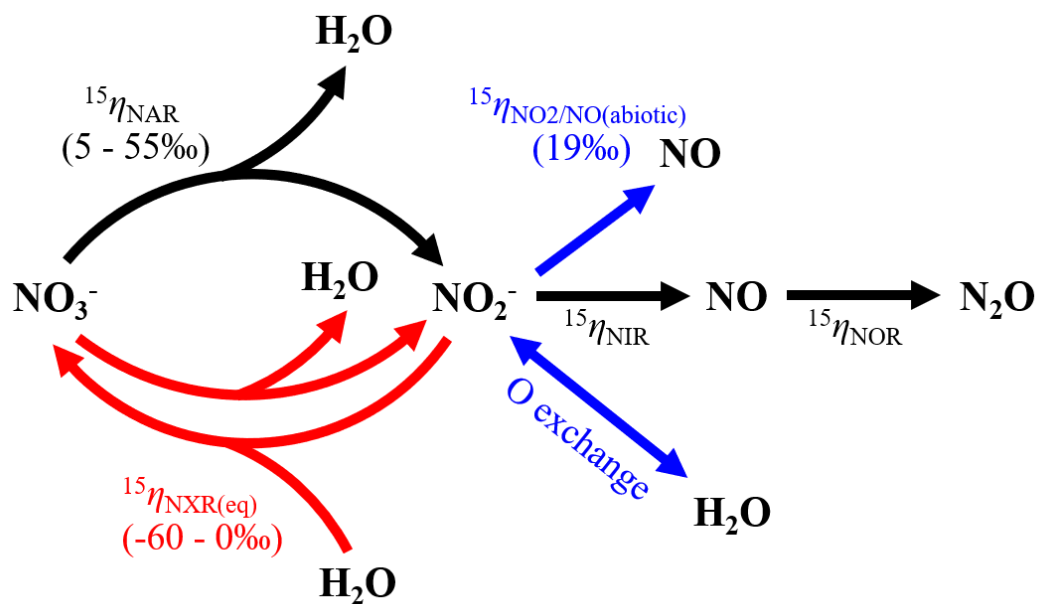
1130 Figure 4. $\delta^{15}\text{N-NO}$ as a function of $\delta^{15}\text{N-NH}_4^+$ in the oxic and hypoxic incubations.



1131

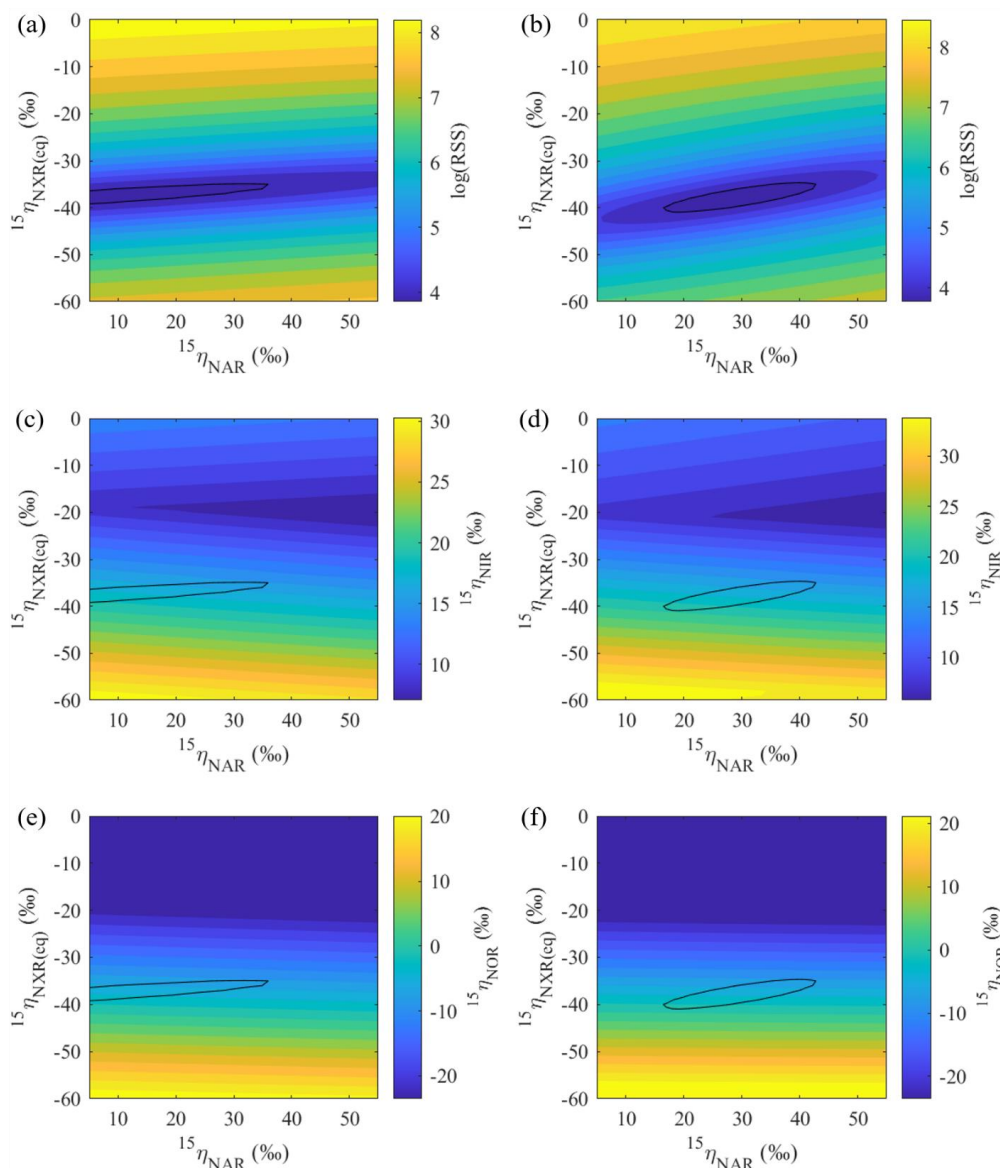
1132 Figure 5 (a) Net NO production rate ($f_{\text{NO-abiatic}}$) of the NO_2^- -amended sterilized soil as a function of time.

1133 (b) Plot of the natural logarithm of $f_{\text{NO-abiatic}}$ versus time showing first-order decay of $f_{\text{NO-abiatic}}$.



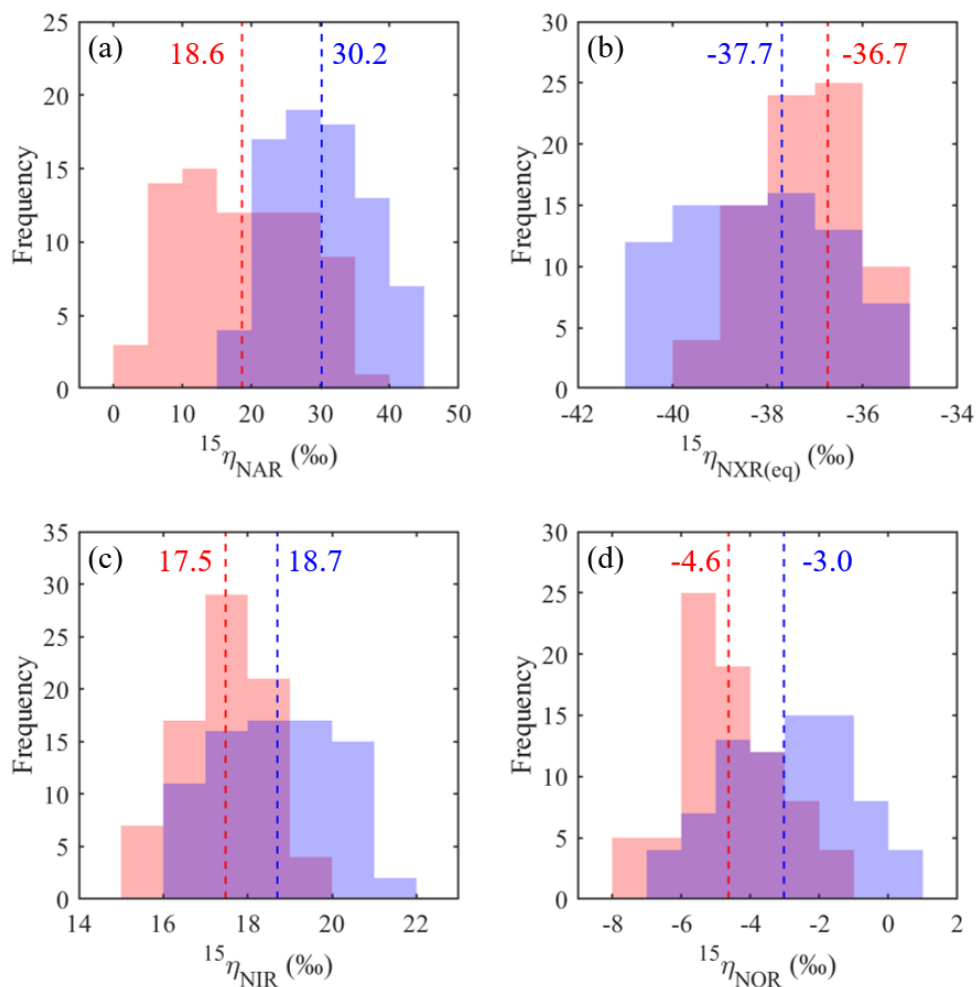
1134

1135 Figure 6. Model structure of co-occurring denitrification and NO_2^- re-oxidation and associated N isotope
1136 effects.



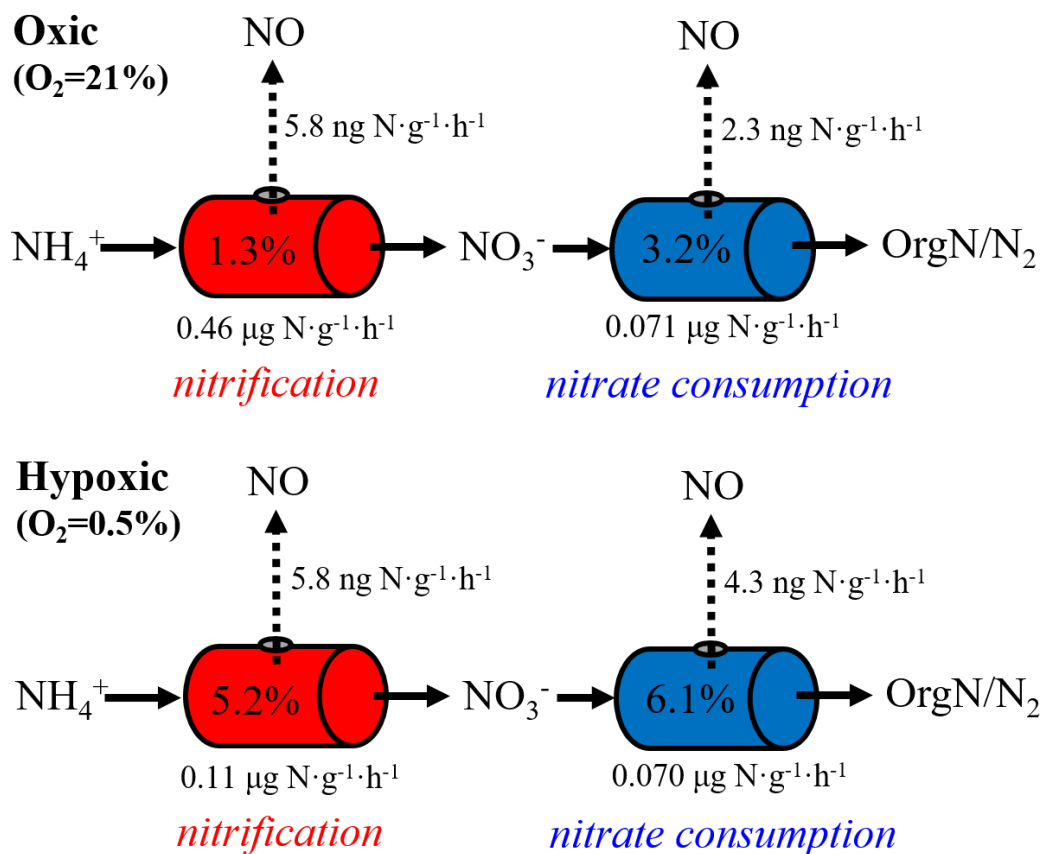
1137

1138 Figure 7. Contour maps showing variations in error-weighted residual sum of squares (RSS) between simulated and
1139 measured $\delta^{15}\text{N}$ values, modeled $^{15}\eta_{\text{NIR}}$, and modeled $^{15}\eta_{\text{NOR}}$ as a function of prescribed $^{15}\eta_{\text{NAR}}$ and $^{15}\eta_{\text{NXR}}$ under the
1140 ‘no exchange’ (a, c, and e) and ‘complete exchange’ (b, d, and f) model scenarios. Bold contour lines encompass the
1141 best-fit models defined by the lower 2.5th percentile of the error-weighted RSS.



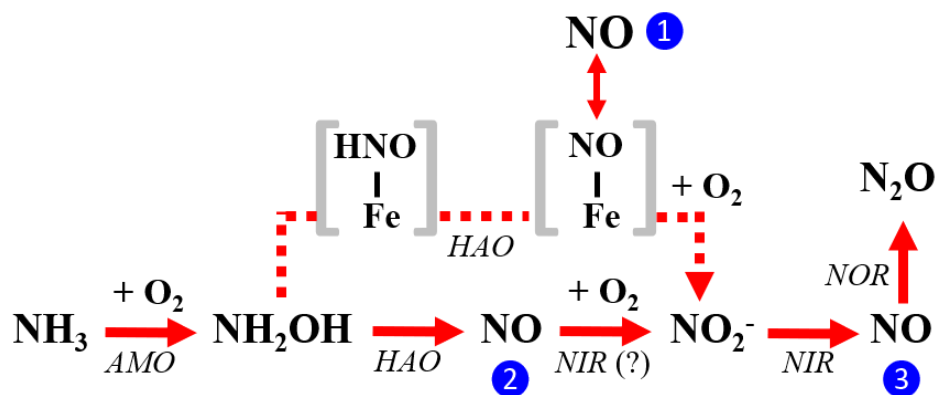
1142

1143 Figure 8. Frequency distributions of the best-fit $^{15}\eta_{\text{NAR}}$ (a), $^{15}\eta_{\text{NXR(eq)}}$ (b), $^{15}\eta_{\text{NIR}}$ (c), and $^{15}\eta_{\text{NOR}}$ (d) under the 'no
1144 exchange' (red) and 'complete exchange' (blue) model scenarios. Dashed vertical lines denote the RSS-weighted
1145 mean $^{15}\eta$ values from the best-fit models under the two model scenarios.



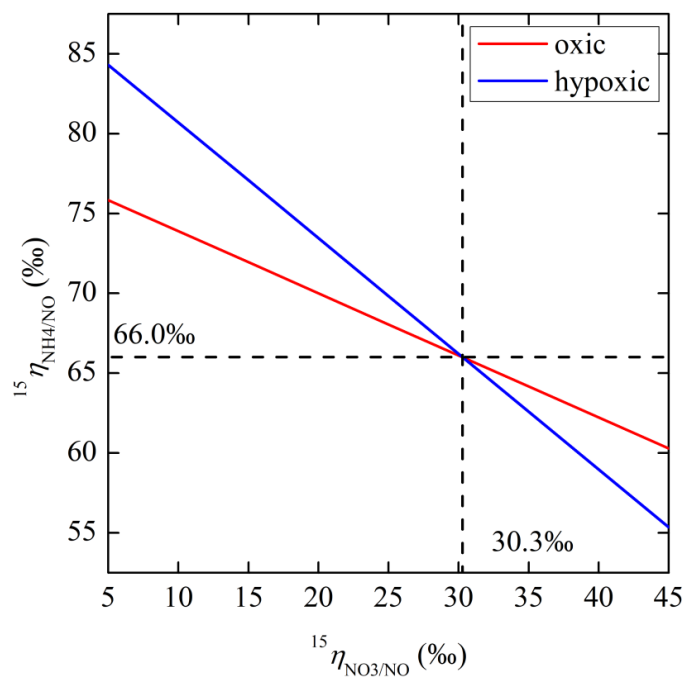
1146

1147 Figure 9. “Hole-in-the-pipe” illustration of NO production from gross nitrification and NO_3^- consumption under oxic
 1148 and hypoxic conditions. “OrgN” denotes organic nitrogen.



1149

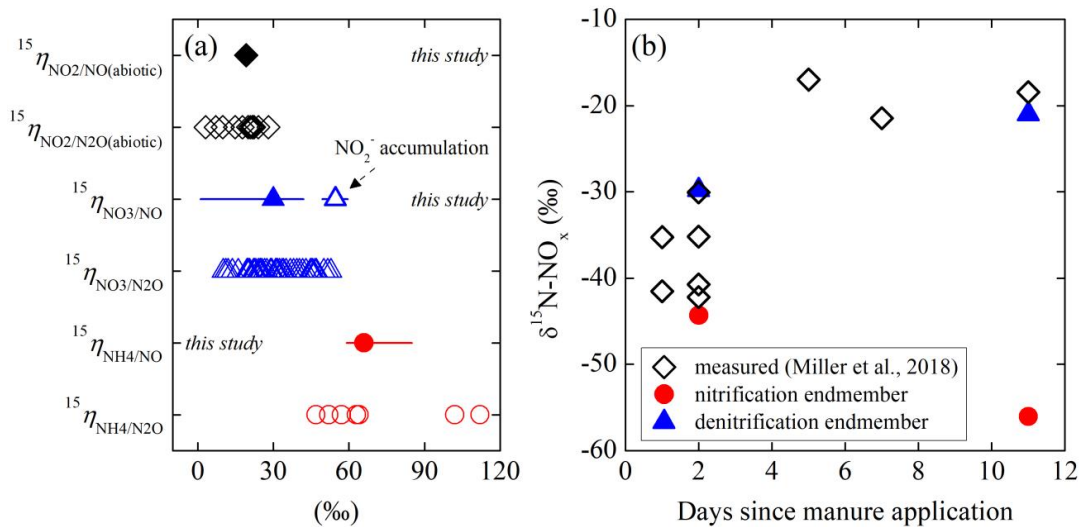
1150 Figure 10. Three enzymatic pathways for NO production during NH₃ oxidation to NO₂⁻ by AOB: the
 1151 ‘NH₂OH obligatory intermediate’ pathway indicated by blue circle (1), the ‘NH₂OH/NO obligatory
 1152 intermediate’ pathway indicated by blue circle (2), and ‘nitrifier-denitrification’ pathway indicated by
 1153 blue circle (3). Square brackets enclose proposed enzyme-bound intermediates [HNO-Fe] and [NO-Fe] of
 1154 the ‘NH₂OH obligatory intermediate’ pathway. The role of AOB-encoded nitrite reductase (NIR) in
 1155 catalyzing NO oxidation to NO₂⁻ in the ‘NH₂OH/NO obligatory intermediate’ pathway is hypothetical.



1156

1157 Figure 11. Relative magnitude of net N isotope effects for NO production from NH_4^+ oxidation ($^{15}\eta_{\text{NH}_4/\text{NO}}$)

1158 and NO_3^- consumption ($^{15}\eta_{\text{NO}_3/\text{NO}}$) in the oxic and hypoxic incubations.



1159

1160 Figure 12. (a) Comparison of net isotope effects for NO production estimated in this study to net isotope
 1161 effects for N₂O production reported in the literature. (b) Comparison of in situ $\delta^{15}\text{N}$ of NO_x emission from
 1162 a manure-fertilized soil (reported by Miller et al. (2018)) to nitrification and denitrification $\delta^{15}\text{N}$ -NO
 1163 endmembers derived using the estimated net isotope effects for NO production in the oxic and hypoxic
 1164 incubations.